

Assessment, Development and Validation of Wind Turbine Rotor Noise Prediction Codes

Department of
Wind Energy
Master Report

Oriol Ferret Gasch

DTU Wind Energy Master Thesis M-0053

Monday 30th June, 2014



Title: Assessment, Development and Validation of Wind Turbine Rotor Noise Prediction Codes

Author: Oriol Ferret Gasch

Department: European Wind Energy Master - EWEM

Summary (max. 2000 characters):

Wind turbine noise has become an important issue when developing on-shore wind farms as turbines have scale up rapidly in the latest decades. The interest of this project is focused on the characterization and modelling of noise as a source based on the specific physics from wind turbines. A dedicated evaluation of wind turbine noise measurements is carried out in order to know more about the behaviour of it in front different operational conditions. Such study assists to understand trends that can be introduced to improve existing semi-analytical or empirical aeroacoustic models, typically used, in wind turbine noise predictions. The result, enhanced aeroacoustic models with an overall uncertainty reduced when compared to measurements. Therefore, these reliable models can be used for future predictions when scoping new rotors or for performance analysis, i.e. development of low-noise strategies.

Monday 30th June, 2014

Project Period:

2014.02.01 2014.06.30

ECTS:

30

Education:

Master of Science

Field:

Wind Energy

Supervisor:

Helge Aagaard Madsen

Supervisor (external):

Daniele Ragni

Stefan Oerlemans

Remarks:

This report is submitted as partial fulfillment of the requirements for graduation in the above education at the Technical University of Denmark.

Contract no.: -

Project no.:

DTU Wind Energy Master Thesis M-0053

Sponsorship: DTU-Risø

TUD-DUWIND

Siemens Wind Power A/S

Front page:

Horizontal axis wind turbines running in Flø, close to Brande kommune, Denmark.

Pages: (74) 216

Tables: (5) 13

References: 69

Danmarks Tekniske Universitet

DTU Vindenergi

Nils Koppels Allé

Bygning 403

2800 Kgs. Lyngby

www.vindenergi.dtu.dk

Assessment, Development and Validation of Wind Turbine Rotor Noise Prediction Codes

Oriol Ferret Gasch

Monday 30th June, 2014



Assessment, Development and Validation of Wind Turbine Rotor Noise Prediction Codes

MASTER OF SCIENCE THESIS

For obtaining the degree of Master of Science in Wind Energy
Engineering at Technical University of Denmark and in Aerospace
Engineering at Delft University of Technology.

Oriol Ferret Gasch

Monday 30th June, 2014

European Wind Energy Master - EWEM
DUWIND - Delft University of Technology
Risø - Denmark Technical University
Siemens Wind Power A/S



Risø DTU



Copyright © Oriol Ferret Gasch
All rights reserved.

EUROPEAN WIND ENERGY MASTER - EWEM
OF
ROTOR DESIGN TRACK

The undersigned hereby certify that they have read and recommend to the European Wind Energy Master - EWEM for acceptance a thesis entitled “**Assessment, Development and Validation of Wind Turbine Rotor Noise Prediction Codes**” by **Oriol Ferret Gasch** in partial fulfillment of the requirements for the degree of **Master of Science**.

Dated: Monday 30th June, 2014

Supervisor:

Dr.ir. H.Aa. Madsen, Supervisor of DTU-Risø

Supervisor:

Dr.ir. D. Ragni, Supervisor of TU Delft

Supervisor:

Dr.ir. S. Oerlemans, Supervisor of Siemens Wind Power A/S

Reader:

Prof.dr. G.J.W. van Bussel, Head of Wind Energy Group at TU Delft

Summary

This MSc Thesis focuses on the study and improvement of state-of-the-art aeroacoustic models for wind turbine applications.

The analysis and understanding of wind turbine measurements performed under specific operational conditions has provided enough evidences about the weaknesses of such models, and therefore, reasons to introduce modifications that allow reducing the overall uncertainty in terms of level and spectrum.

Based on that, modifications have been introduced in existing state-of-the-art aeroacoustic methods. Having the measurements and the operational settings; i.e. rotor speed and pitch angle, the validation process of such models has been possible, in an effort of reducing the overall uncertainties. Both frequency spectrum and level have been predicted, analysed and improved in order to reduce the high uncertainty typically reported in these models.

Besides covering the physical part of the noise mechanism and modelling, this project has also studied the noise performance of a wind turbine. By having a reliable acoustic model, it has been possible to investigate and design new operational settings that allow running a turbine under specific noise constraints (i.e. low-noise modes), by optimising power production. The results of this analysis, if consistent, would be evaluated in real field conditions in order to validate the models.

Acknowledgements

This thesis concludes the project that I decided to start, exactly 2 years ago, when the EWEM board accepted my application as a valid candidate for the first cohort of the European Wind Energy Master. I would first like to thank the EWEM board itself for giving me the chance of participating in it. Special thanks to Dr. Carlos José Simão Ferreira and Dr. Jens Nørkær Sørensen as main coordinators of the programme at TU Delft and DTU respectively, where I have been studying during these 2 years. To them, I wish my best for the success of this programme in the future, and this first thesis should become the predecessor of many more that will follow to strengthen cooperation amongst wind energy research institutes.

I would also like to thank Dr. Helge Aagaard Madsen and Dr. Daniele Ragni, being my supervisors from DTU-Risø and TU Delft-DUWIND for this project. Although it has not been easy, as the three of us we have been allocated it in different places, we have been always able to find a meet as regular as possible during the development of this project. I would like to thank them for the chance they have given me to discuss my ideas and listen from their experience and advice. I must say that it has been a pleasure to work with them.

I would also like to thank Siemens Wind Power A/S for having allowed me to perform this project with them, and specially, to Dr. Stefan Oerlemans, who has been my supervisor at Siemens. Being one of the key experts in the area of aeroacoustics, it has been a great pleasure to work and learn from him along the development of this project. Also thanks to, Peter Fuglsang, head of blades department, and Dr. Alex Loeven, team lead of blades upgrades department, when they decided to invest on me more than 1 year ago to carry out this project. The rest of the members of this team also deserve my most sincere thanks, as they contributed in the success of it. It has been a pleasure to work with all of them.

Finally, but not the least, to my family and friends who supported me during these two years, although they have had to do it, most of the time, from the distance. And to my girlfriend, Irene Merdian, who enlightened and supported me most during the development of it.

Brande, Denmark
Monday 30th June, 2014

Oriol Ferret Gasch

Contents

Summary	v
Acknowledgements	vii
List of Figures	xii
List of Tables	xiii
Nomenclature	xv
1 Introduction	1
1.1 Aim of the Project	1
1.2 Scope of the Project	2
1.3 Motivation of the Project	3
1.3.1 Wind Power: Current Status	3
1.3.2 The Challenge for Onshore Installations: Wind Turbine Noise . . .	7
1.4 Structure of the Project	9
2 State of the Art	11
2.1 Theoretical Aeroacoustics Research	11
2.2 Semi-empirical and Experimental Aeroacoustics	14
2.3 Computational Aeroacoustics methods, CAA	16
3 Aeroacoustics Modelling	19
3.1 Lighthill Acoustic Analogy	19
3.2 Ffowcs, Hall and Hawkings Acoustic Analogy	21
3.3 Turbulent Boundary Layer Trailing Edge Noise, TBL-TE	22
3.3.1 Trailing Edge Noise - BPM Model	23

3.3.2	Trailing Edge Noise - TNO Model	30
3.4	Turbulent Inflow Noise	35
3.4.1	Amiet's Turbulence Inflow Noise Model	36
3.4.2	Extending Amiet Turbulence Inflow Model for Cambered Airfoils	41
4	Analysis of Wind Turbine Noise Measurements	43
4.1	Wind Turbine Steady Performance	43
4.2	Sound Power Level Experimental Measurements	44
4.3	Sound Power Level Measurements Evaluation	46
5	Evaluation, Validation and Improvement of Aeroacoustics Models	47
5.1	Introduction to Wind Turbine Prediction	47
5.2	Evaluation and Improvement of Aeroacoustics Models Against Measurements	49
6	Design of Low-Noise Optimised Control Settings	51
6.1	Noise and Power Performance Spaces	51
6.2	Validating Low-Noise Settings with Field Measurements	52
7	Research Conclusions	55
7.1	Main Contributions of this Thesis	55
7.2	Suggestions for Further Research	57
	References	59
A	Octave Bands	65
A.1	Definition	65
A.2	Octave Band Conversion	66
B	BPM model. Detailed Formulation	69
B.1	Turbulent Boundary Layer Trailing Edge Noise, TBL-TE	69
B.2	Turbulent Boundary Layer - Separation Stall Noise, TBL-SS	72
B.3	Laminar Boundary Layer Vortex Shedding Noise, LBL-VS	72
B.4	Trailing Edge Bluntness Vortex Shedding Noise, LBL-VS	73

List of Figures

1.1	Gantt Chart. Planning of main tasks to be accomplished within the frame of this project	3
1.2	Overview of different energy sources used in Europe a) at the end of 2000, b) at the end of 2013	4
1.3	Wind power installations in Europe during the period 2000-2013. Data has been released by European Wind Energy Association (EWEA). a) Cumulative installations, b) annual installations showing the fraction between onshore and offshore installations	4
1.4	Wind turbine radiating noise towards a nearby dwell	7
2.1	Directivity patterns of linear acoustic singularities; a) monopole, b) dipole, c) quadrupole	12
2.2	Localisation of noise sources. a) Gamesa 0.85 MW - 58.0, Zaragoza (ES), b) General Electric 2.3 MW - 94.0, Wieringermeer (NL), by courtesy of S. Oerlemans [57]	16
3.1	Trailing edge directivity patterns on a semi-infinite flat plate	22
3.2	Sketch of turbulent boundary layer trailing edge noise, TBL-TE	24
3.3	Sketch of turbulent boundary layer separation stall noise, TBL-SS	26
3.4	Sketch of Turbulent boundary layer - tip vortex formation noise, TBL-TV	27
3.5	Sketch of the span wise extension at the tip region	27
3.6	Sketch of trailing edge bluntness vortex shedding noise, TEB-VS	29
3.7	Trailing edge noise mechanism based on TNO model. Sketch based on M. Kamruzzaman [39] research work	30
3.8	Sketch of turbulent inflow noise mechanism	36
4.1	Result of a steady performance calculation. a) Power curve, b) triangle of velocities	44
4.2	Location of the microphone that records wind turbine noise. a) Sketch extracted from IEC-61400-11, b) microphone in real field conditions	45

4.3	Example of a standard sound power level spectra from a wind turbine measurement	45
5.1	Sketch of a blade with their corresponding noise sources distributed along the spanwise direction for a defined number of sections	48
5.2	Representation of xNoise sound power level modes. a) Sound power level is assessed directly on the blades (red spots) and considered equal for each blade. b) Sound pressure level is assessed at a receiver position, adding the contribution of each blade and propagating it back (dash bold line) to hub height (green spot)	48
6.1	Annual energy production calculation	52

List of Tables

1.1	Wind power annual installations (MW) in European Union (EU-28) and European Free Trade Association (EFTA) countries since 2009 until the end of 2013 based on data released by the European Wind Energy Association (EWEA)	5
1.2	Wind power cumulative installations (MW) in other countries since 2010 until the first half of 2013. Data has been release by the World Wind Energy Association (WWEA)	6
1.3	Wind turbine noise regulations for different countries. All the values are expressed in sound pressure level with $p_0 = 2 \cdot 10^{-5}$ [Pa]. Data is based on K. Fowler <i>et al.</i> [28]	8
A.1	Octave bands	66
A.2	Conversion from one-third octave band levels to one octave band levels. .	67

Nomenclature

Latin Symbols

a	Axial induction coefficient	[-]
AEP	Annual Energy Production	[MWh]
C_f	Skin friction coefficient	[-]
c_0	Speed of sound	[m/s]
C_p	Power coefficient	[-]
C_t	Thrust coefficient	[-]
d	Span length	[m]
D	Rotor diameter	[m]
$F_{U,\text{Rayleigh}}$	Rayleigh cumulative density function	[-]
\mathbf{G}_1	Spectrum function for LBL-VS	[dB]
\mathbf{G}_2	Spectrum function for LBL-VS	[dB]
\mathbf{G}_3	Spectrum function for LBL-VS	[dB]
\mathbf{G}_4	Spectrum function for TEB-VS	[dB]
\mathbf{G}_5	Spectrum function for TEB-VS	[dB]
H	Hub height	[m]
I	Acoustic intensity	[kg/s ³]
k_e	Wave number of energy-containing eddies	[1/m]
k_T	Turbulence kinetic energy	[m/s]
k_1	Longitudinal wavenumber	[1/m]
k_3	Lateral wavenumber	[1/m]
l_m	Turbulent mixing length	[m]

N_B	Number of blades	[-]
P	Power	[W]
$f_{U,\text{Rayleigh}}$	Rayleigh probability density function	[-]
r_e	Slant distance between source and receiver	[m]
RH	Relative humidity	[%]
\mathbf{S}_{FF}	Far field spectrum	[Pa ² /Hz]
\mathfrak{S}	Sears function for compressible flow	[-]
p_{ij}	Stress tensor	[kg/ms ²]
A	Effective rotor area	[m ²]
T	Air temperature	[K]
T_{ij}	Lighthill stress tensor	[kg/ms ²]
U_1	Streamwise mean velocity	[m/s]
U_c	Convective velocity of turbulent eddies	[m/s]
U_e	Convective velocity at the edge of the boundary layer edge	[m/s]
U_I	Total inflow speed-relative speed seen by a blade section	[m/s]
U_s	Power curve converted wind speed	[m/s]
$\overline{u_2^2}$	RMS of Vertical velocity fluctuations	[m ² /s ²]
U	Wind speed at hub height	[m/s]
u^*	Friction velocity	[m/s]
U_z	Measured wind speed at a given height	[m/s]
u_i	Velocity vector	[m/s]
\mathbf{x}	Source location	[m]
x_2	Vertical coordinate	[m]
\mathbf{y}	Receiver location	[m]
z_0	Roughness length	[m]

Greek Symbols

Φ_m	Moving axis spectrum	[m/s]
Φ_{22}	Vertical velocity fluctuations spectrum	[m/s]
λ	Tip speed ratio	[-]
Λ_2	Vertical integral turbulence length	[m]
μ	Dimensionless blade radius	[-]
ν	Kinematic viscosity	[m ² /s]
Ω	Rotor speed	[rad/s]
$\bar{\alpha}$	Atmospheric absorption coefficient	[dB/100 m]
$\bar{\omega}$	Reduced frequency, $\omega c/(2U)$	[-]
θ_p	Pitch angle	[rad]

θ_t	Geometrical twist angle	[rad]
α	Angle of attack	[rad]
δ	Boundary layer thickness	[m]
δ^*	Boundary layer displacement thickness	[m]
δ_p^*	Pressure side boundary layer displacement thickness	[m]
δ_s^*	Suction side boundary layer displacement thickness	[m]
κ	Von Karman constant	[-]
ν_t	Turbulent viscosity	[m ² /s]
Ψ_e	Trailing edge spanwise directivity angle	[deg]
ρ	Density	[kg/m ³]
θ_e	Trailing edge chordwise directivity angle	[deg]
θ	Boundary layer momentum thickness	[m]

Abbreviations

AEP	Annual Energy Production
AoA	Angle of Attack
BG	Background noise
LBL-VS	Laminar Boundary Layer Vortex Shedding Noise
SWP	Siemens Wind Power
TBL-SS	Turbulent Boundary Layer Separation Stall Noise
TBL-TE	Turbulent Boundary Layer Trailing Edge Noise
TBL-TV	Turbulent Boundary Layer Tip Vortex Noise
TEB-VS	Trailing Edge Bluntness Vortex Shedding Noise

Chapter 1

Introduction

Wind turbine noise has gained importance as wind turbines have scaled up for more energy production.

This introductory chapter provides a quick overview to the reader of why wind turbine noise has become a concern on onshore installations as wind energy grows exponentially all over the world.

1.1 Aim of the Project

The aim of this project is to assess the validity of existing aeroacoustic models applied to wind turbines with respect to field measurements, improve them and use them, later, for designing new low noise strategies.

1.2 Scope of the Project

This research project is conducted within the collaboration of DTU, TU Delft and Siemens Wind Power A/S. The latter party provides field measurements to carry out this research.

The scope of this project has been planned to:

- Gather internal and external noise measurements for different turbines: standard IEC measurements and long-term measurements under standard and special control settings: Pitch angle and rotor speed.
- Analyse and post-process measurements (background noise, mechanical noise, microphone misalignment, wind shear, etc.), and determine turbine settings. Establish trends in rotor noise as a function of wind turbine operation parameters and meteorological conditions, if applicable.
- Evaluate SWP prediction method against noise measurements for different turbines. Consider overall noise levels as function of wind speed or power, but also spectral characteristics.
- Describe different publicly available rotor noise prediction methods, and assess how the SWP method can be improved. Describe the assumptions used in prediction methods for different mechanisms (trailing edge noise, inflow turbulence noise, etc.) and assess their validity, if applicable.
- Develop a methodology or algorithm for designing new low-noise control settings that consider operational constraints while maximising energy yield. Apply such methodology to generate new settings.
- Validate field measurements for a test case based on new low-noise control settings.

On the other hand, the following aspects are out of the initial scope:

- There **will not** be a detailed description of wind turbine BEM theory, but emphasised when necessary. The reader must be, somehow, familiarised with wind turbine fundamentals.
- Computational Aeroacoustic methods (CAA) **will not** be applied but their characteristics mentioned.
- Use of advance wind turbine noise measurement techniques, i.e. array measurements, **are totally discarded**.

The project planning is also displayed in Figure 1.1 to provide a visual description of how this project has been carried out.

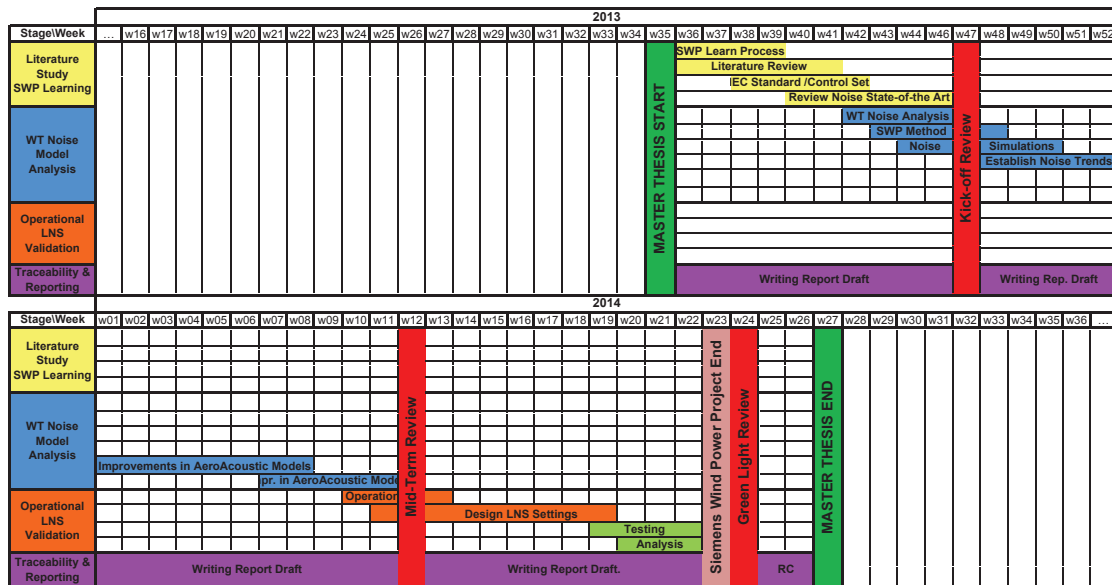


Figure 1.1: Gantt Chart. Planning of main tasks to be accomplished within the frame of this project

1.3 Motivation of the Project

1.3.1 Wind Power: Current Status

Wind energy, undoubtedly, has become one of the renewable energy sources that has undergone a progressive and steady increase during the last decades¹. On the contrary, traditional and most polluted sources of energy such as fuel oils, coal or nuclear have decreased in a slower pace as a result of the existent high demand of energy from all over the world.

The good news is that wind power systems become more efficient as turbines enlarge substantially their sizes in order to capture more energy from the wind. Manufacturers along with research institutes specialised in wind energy have improved the know-how, being able to introduce constantly new technology in the quest for efficiency improvement and energy mass production.

Figure 1.2 shows how wind energy has started to play a role within the most consume energy sources.

¹ Source from The European Wind Energy Association EWEA: <http://www.ewea.org/statistics/>

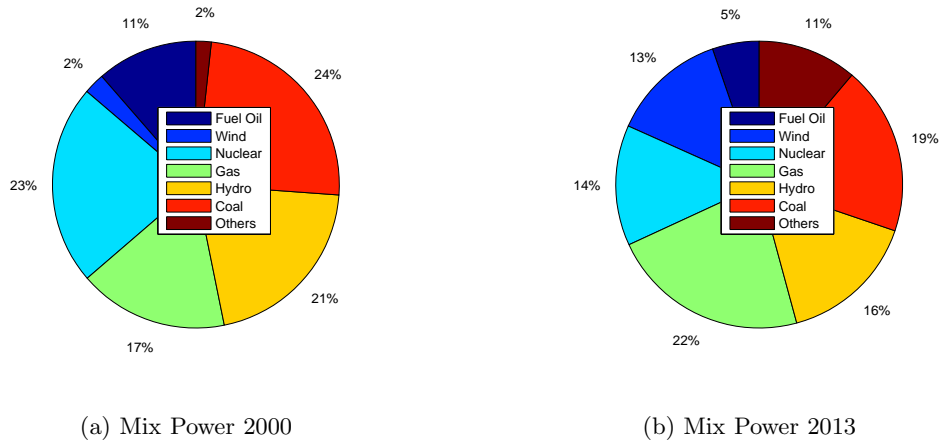


Figure 1.2: Overview of different energy sources used in Europe a) at the end of 2000, b) at the end of 2013

While at the beginning of the 21th century, wind energy just meant only a 2% of the total energy produced in Europe, nowadays, it represents an important part of the energy pie when compared it with respect to traditional sources nuclear, coal, and fuel oil.

In 2011, wind energy becomes comparable to nuclear or hydro in Europe. In some countries, like Spain, wind power even beats nuclear for the first time². While in others, such as Denmark, there are ambitious prospectives in the current long term targets by being only powered by wind energy.

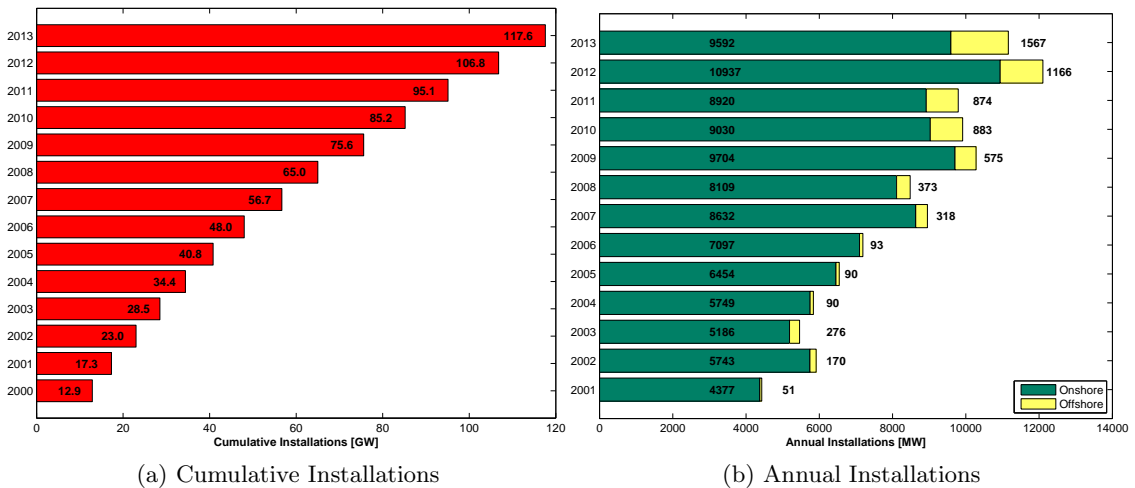


Figure 1.3: Wind power installations in Europe during the period 2000-2013. Data has been released by European Wind Energy Association (EWEA). a) Cumulative installations, b) annual installations showing the fraction between onshore and offshore installations

Nowadays, more than 25% of the energy consumption in Denmark is coming from wind

²Source from Red Eléctrica de España: <http://www.ree.es/en>

energy, a percentage that is planned to hit 50% by the end of 2020³.

Table 1.1: Wind power annual installations (MW) in European Union (EU-28) and European Free Trade Association (EFTA) countries since 2009 until the end of 2013 based on data released by the European Wind Energy Association (EWEA)

EU-28		2009	2010	2011	2012	2013
Austria	AT	995	1,014	1,084	1,377	1,684
Belgium	BL	563	886	1,078	1,375	1,651
Bulgaria	BG	177	500	516	674	681
Croatia	HR	28	89	131	180	302
Cyprus	CY	0	82	134	147	147
Czech Republic	CZ	192	215	217	260	269
Denmark	DK	3,465	3,749	3,956	4,162	4,772
Estonia	EE	142	149	184	269	280
Finland	FI	147	197	199	288	448
France	FR	4,574	5,970	6,807	7,623	8,254
Germany	DE	25,777	27,191	29,071	30,989	33,730
Greece	GR	1,087	1,323	1,634	1,749	1,865
Hungary	HU	201	295	329	329	329
Ireland	IE	1,310	1,392	1,614	1,749	2,037
Italy	IT	4,849	5,797	6,878	8,118	8,551
Latvia	LV	28	30	48	60	62
Lithuania	LT	91	163	179	263	279
Luxembourg	LU	35	44	45	58	58
Malta	MT	0	0	0	0	0
Netherlands	NL	2,215	2,269	2,272	2,391	2,693
Poland	PL	725	1,180	1,616	2,496	3,390
Portugal	PT	3,535	3,706	4,379	4,596	4,724
Romania	RO	14	462	982	1,905	2,599
Slovakia	SK	3	3	3	3	3
Slovenia	SI	0	0	0	0	2
Spain	ES	19,160	20,623	21,674	22,784	22,959
Sweden	SE	1,560	2,163	2,899	3,582	4,470
United Kingdom	GB	4,245	5,204	6,556	8,649	10,531
Total EU-28		75,118	84,696	94,485	106,076	116,770
EFTA		2009	2010	2011	2012	2013
Iceland	IS	0	0	0	0	2
Liechtenstein	LI	0	0	0	0	0
Norway	NO	431	441	537	703	768
Switzerland	CH	18	42	46	50	60
Total EFTA		449	483	583	753	830
Total EU-28 + EFTA		75,567	85,179	95,068	106,829	117,600

However, not only Spain and Denmark have joined to the train of renewable energy, there

³See Denmark.dk, the Official Web of Denmark, <http://denmark.dk/en/green-living>

is a worldwide commitment to reduce CO2 emissions, and wind energy it is one of the main drivers.

Other renewable sources not shown in Figure 1.2 include ocean power, photovoltaic, concentrated solar power, biomass, etc. Those are also gaining weight amongst other traditional energy sources, but still, each of them is not determining an impact as wind power does. Nevertheless, there is still a lot of potential to be extracted from renewable sources.

Back to Europe, Figure 1.3 shows some interesting aspects. Regardless the current economic turmoil period that is hitting Europe as a result of the financial crisis from 2008, wind energy installations have not stopped to increase year after year. Figure 1.3a shows how the cumulative installations increase year after year, whether traditional wind energy countries such as Germany, Spain or Denmark increase their current capacity or new players decide to invest in wind, i.e. Great Britain, Sweden or France.

Table 1.1 provides a real overview of the cumulative installations since 2009 until the end of 2013 of all the countries within the European Union + EFTA. The reader can realise the impact of wind energy in Europe. By the end of 2013, all the countries except Malta (MT) and Lichtenstein (LI) registered installed MegaWatts coming from wind energy. Besides, the trend from the last 5 years reveals a substantial increase on installations in most of the European countries, being Europe, the main worldwide producer of wind energy.

Table 1.2: *Wind power cumulative installations (MW) in other countries since 2010 until the first half of 2013. Data has been release by the World Wind Energy Association (WWEA)*

Country		2010	2011	2012	2013
China	CN	44,733	62,364	75,324	80,824
USA	US	40,180	46,919	60,007	60,009
India	IN	13,065	15,880	18,321	19,564
Canada	CA	4,008	5,265	6,201	6,578
Australia	AU	1,880	2,226	2,584	3,059
Brazil	BR	930	1,429	2,507	2,788
Japan	JP	2,304	2,501	2,614	2,655
:	:	:	:	:	:
Total World		199,739	237,717	282,275	296,255

However, this is not a unique trend in Europe; other countries in the rest of world are also aligned in the same direction. Table 1.2 shows the main countries out of European borders that are also strong in wind energy. Most of them belong to the BRIC countries⁴ such as China whose installations grew exponentially in the past 5 years becoming the first country in the world with most MW installed. US are lagging behind due to the new regulations regarding wind energy fares. Even though, it doubles Germany capacity according to Table 1.1.

Nevertheless, the number of installations in these countries must be massive in order to reach the same levels as Spain reported last year or the objectives of Denmark since the

⁴BRIC stands for the emergent economies Brazil, Russia, India and China

number of households to be fed is way larger compared to European countries, where the number of inhabitants per country is usually smaller.

1.3.2 The Challenge for Onshore Installations: Wind Turbine Noise

Since now, the overall status of wind power has been mentioned, but nothing regarding why wind turbine noise is a problem of social concern. For that, it is interesting to analyse Figure 1.3b.

What Figure 1.3b shows is basically the overall ratio of onshore and offshore installations, in this case, in Europe. Offshore installations have increased substantially in the last decades, mainly due to, a great number of advantages (installations, logistics, higher winds, etc.). Denmark has been always the pioneer, and recently Germany and UK joined in the conquest of overseas wind power thanks to the conditions offered by the North and Baltic sea respectively, where most of the offshore installations are concentrated.⁵

Nevertheless offshore installations are costly and they imply a higher investment risk compared to onshore installations, where the market is far more consolidated as Figure 1.3b shows. It is in onshore where wind turbine noise becomes a problem.

Indeed, wind farms are usually installed based on an accurate or approximated study of the wind resource in a certain area, but the design is always constrained by socio-economic and environmental aspects. While in some regions, it is easy to erect turbines in isolated areas, a vast majority of them are concentrated close to inhabited areas, as transportation is easier due to developed infrastructures and energy losses are reduced.

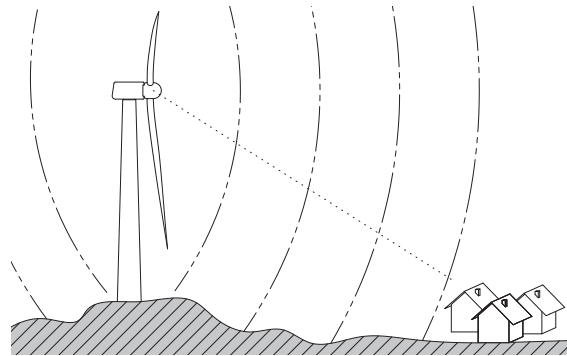


Figure 1.4: Wind turbine radiating noise towards a nearby dwell

Nevertheless, wind turbine noise is a reality, it exists, and its effects can be important depending on the distance between dwells and turbines, but also depending on wind direction. Wind turbine noise is not as extreme as an aircraft flying over the proximities of an airport, but the source is static and repetitive, emitting noise in a vast range of frequencies. These combined features make wind turbine noise one of the most annoying noise sources for those who are exposed. Therefore, it can generate psychological effects on people.

⁵These seas are shallow, meaning that foundations and substructures are easy to install than in other deeper seas, i.e. Mediterranean. For further information, check "Infographic on the 2013 offshore statistics", by EWEA <http://www.ewea.org/statistics/>

In general, such effects can be classified into three general categories according to a study from A.L. Rogers *et al.*[62]:

- Subjective effects including annoyance, nuisance and dissatisfaction.
- Interference with activities such as sleep and hearing.
- Physiological effects such as anxiety or hearing loss.

For that reason, some European and non-European countries possess regulations regarding industrial noise, others, they even created specific rules for wind turbine noise. Table 1.3 summarizes accurately the differences between countries in regard wind turbine noise limits.

Table 1.3: Wind turbine noise regulations for different countries. All the values are expressed in sound pressure level with $p_0 = 2 \cdot 10^{-5}$ [Pa]. Data is based on K. Fowler *et al.* [28]

Country	Noise Metric	Rural	Residential	Others
BE - F	$L_{A,eq}$ @ 95% RP [dB(A)]	Day: 48	Day: 44	Day: 48
		Night: 43	Night: 39	Night: 43
BE - W	$L_{A,eq}$ @ All U [dB(A)]	45	45	45
CA	$L_{A,eq}$ [dB(A)]	Night: 40	Night: 40	Night: 40
DK	L_r @ 6 m/s [dB(A)]	42	37	37
	L_r @ 8 m/s [dB(A)]	44	39 @	39 @
FR	L_r @ All U [dB(A)]	BG +5 dB(A)		
DE	L_r @ All U [dB(A)]	Day: 60	Day: 50-55	Day: 60
		Night: 45	Night: 35-40	Night: 45
NL	L_{den} [dB]	47		
	L_{night} [dB]	41		
NZ	$L_{A,90}$ [dB(A)]	35 or BG+5 dB(A)	40 or BG + 5 dB(A)	40 or BG + 5 dB(A)
NO	L_{den} [dB]	45	45	45
AU	$L_{A,90}$ [dB(A)]	35 or BG+5 dB(A)	40 or BG + 5 dB(A)	40 or BG + 5 dB(A)
SE	$L_{A,eq}$ @ 8 m/s [dB(A)]	35	40	40
GB	$L_{A,90}$ [dB(A)]	Day: BG + 5 dB(A) + Lower Limit 40 dB(A)		
		Night: BG + 5 dB(A) + Lower Limit 43 dB(A)		

All wind speeds from Table 1.3 are referred to 10m height according to IEC-61400-11 [37]. Moreover, the whole range of wind speeds covers from 6 to 10 m/s in case it is not indicated the contrary, i.e. Denmark. In some countries, like UK, it can be extended.

As it can be seen, different noise metrics are used; $L_{A,eq}$, L_r , $L_{A,90}$ or L_{den} ⁶ that provide a constant value from a measurement over a certain period of time.

$${}^6L_{den} = 10 \log_{10} \left(\frac{12 \cdot 10^{L_{day}/10} + 4 \cdot 10^{L_{day}+5/10} + 8 \cdot 10^{L_{night}+10/10}}{24} \right)$$

Those countries that consider wind turbine noise on a background noise basis, BG, introduce more uncertainties when validating new turbines just installed, as BG noise is generated as a result of a bunch of random effects from the surrounding area (forests, wind, cities, etc). Manufacturers must be in charge of providing sound power levels (noise at the source) and make wind turbines quieter. However, Table 1.3 becomes relevant when planning a wind farm installation. For the same noise level more or less turbines are erected in an area as long as they are compliant with existent noise regulations.

As an important outline, the reader must be familiar that independent and incoherent (not in phase) noise sources sum together according to the following addition rule;

$$SWL_{\text{Total}} = 10 \log_{10} \left(\sum_{i=1}^N 10^{SWL_i/10} \right) \quad (1.1)$$

The rule applies either considering sound power level or sound pressure level. Eq.(1.1) is widely used along this document in the following chapters.

Table 1.3 only deals with overall level, but K. Fowler *et al.* [28] also introduce regulations in the spectra. Low frequencies are less attenuated than high frequencies when noise propagates through the atmosphere, therefore some countries apply some limits for low frequencies, i.e. Denmark. The perception of noise with a different peak frequency can be different even at a given overall sound power level.

Therefore, enough reasons have been given to prove that wind turbine noise is a state-of-the-art problem in onshore wind turbines. That is exactly the start-up motivation of this project. From the research point of view, it is relevant to improve the know-how, so that wind turbine noise can be characterised and evaluated based on the performance of a wind turbine. In that sense, noise could be included as another constraint within the design loops.

1.4 Structure of the Project

The structure of this thesis research project follows the milestones set up in previous Section 1.2 when defining the scope of the project.

Each chapter listed below goes together with a small description or guide that helps the reader to understand the whole picture of this project and what each chapter contains, before focusing on a special matter.

- **Chapter I.** Introduction to the project objectives and review of current status of wind energy as a reliable renewable source and justify why wind turbine noise is a current concern.
- **Chapter II.** A review of wind turbine aeroacoustics state-of-the-art is thoroughly carried out, outlining and summarising all the research done so far and mentioning future trends.
- **Chapter III.** This chapter exposes the general theories behind the physical mechanisms that generate wind turbine noise. Several models are described in depth,

providing a clear overview of analytical, semi-empirical and computational methods applied in wind turbine aeroacoustics.

- **Chapter IV.** The thesis focuses first on the analysis and understanding of existing wind turbine measurements. The purpose, basically, is to find some laws that allow describing, in a simple way, how wind turbine noise behaves. The results are used to correct the deficiencies of existing aeroacoustic models when predicting wind turbine noise.
- **Chapter V.** Having understood noise measurements and successfully modelled them using a simple physical model, it is time to analyse the current models. Changes in these models are based on the findings from Chapter IV in order to improve predictions. Besides, it also shows an update of the models, by introducing elements that could not be modelled with existing equations.
- **Chapter VI.** Once the models have been updated, this chapter focuses on low-noise wind turbine control strategies. Basically, the objective is to define new low-noise strategies that could produce more AEP than current ones. So, a methodology is defined by coupling an acoustic model with a power performance model. Therefore, a set of settings for maximum energy yield is expected to be found.
- **Chapter VII.** The conclusions of the whole project are drawn up in this final chapter where the objectives, set up initially, are reviewed in regards the results achieved.

This is an unrestricted version of the original report, which is prescribed by an existent NDA amongst Siemens Wind Power, TU Delft and DTU. For that reason, **Chapters IV, V and VI**, have been accordingly summarized to avoid publishing sensible information.

Detailed or additional information from previous Chapters has been also included in two appendixes; A, B.

Chapter 2

State of the Art

The field of aeroacoustics has become important since the latest 60 years. Experiencing a considerable development and improvement as any other of the current physics or engineering fields where fluid dynamics plays a fundamental role on it, trying to model numerous situations involving fluid interaction with solid surfaces.

Aeroacoustics is that field of fluid dynamics that studies the origin and propagation of pressure fluctuations generated when a flow, especially of turbulent nature, interacts with a solid surface. Although, there are several structures affected by these phenomena, such as buildings, nozzles, etc... The aeroacoustics that are studied along this research project are focused on sounds generated by aerodynamic surfaces present in numerous engineering applications such as propellers, helicopters or wind turbines.

In this chapter, a review of fundamental of aeroacoustics theory applied to airfoils, up to the current state-of-the-art methods are described in order to familiarise the reader into this field, so often, not well-known by the fluid dynamics scientific community.

2.1 Theoretical Aeroacoustics Research

All the research and models developed until recent years starts from the analogy that M.J. Lighthill, [44], [45] derived from the well-known Navier-Stokes equations. Lighthill proposed a derivation starting from the mass and momentum conservation equations for a flow, up to reaching an acoustic analogy that makes possible to solve the aerodynamic sound by using a stationary wave equation.

Lighthill introduces the concept of a turbulent stress tensor which represents the radiation source terms per unit of volume coming from convection, shear and pressure. Those are modelled using an acoustic quadrupole.¹ Normally the influence of the Lighthill stress tensor focuses on small regions of the flow where perturbations could be introduced by

¹In acoustic theory, sources can be modelled using linear combination of singularities made of monopoles, dipoles or quadrupoles.

solid surfaces, in the outer regions, any acoustic fluctuation is quickly damped out by the flow convection.

Kirchhoff reformulated Lighthill analogy by defining a volume where turbulence fluctuations occur. This formulation, only considers the far field solution as a result of the complexity introduced by retarded time evaluation plus the spatial derivatives. In that sense, the role developed by Lighthill's Tensor becomes clearer although the formulation is only valid when there are no solid boundaries. However, neglecting solid surfaces in the generation of noise, it results in one of the main drawbacks of Lighthill's analogy, being only useful for jet noise.

N. Curle [23], proposed the first extension for Lighthill's analogy, being the introduction of static surfaces, and therefore, expanding Lighthill's assumption for unbounded flows. Curle also proved that noise becomes more important when a turbulent flow interacts with a solid surface as a result of the lower Mach numbers and higher Reynolds numbers. J.E. Ffowcs-Williams, L.H. Hall and D.L. Hawkings, included the influence of arbitrary moving surfaces, also known as FH-W model [26] and [27]. The theory is derived similarly from Lighthill analogy over a scattering half plane. The same quadrupole term (Lighthill tensor) plus a dipole and monopole distribution² result out of it (see Figure 2.1). The conclusion of the FH-W model is that solid surfaces become acoustically equivalent to a distribution of monopoles and dipoles of the solid surface whose strength is equal to the local acceleration of the surface and the net force applied on the fluid respectively. In the common literature, the dipole term is often called loading noise, while the monopole term is well-known as thickness noise.

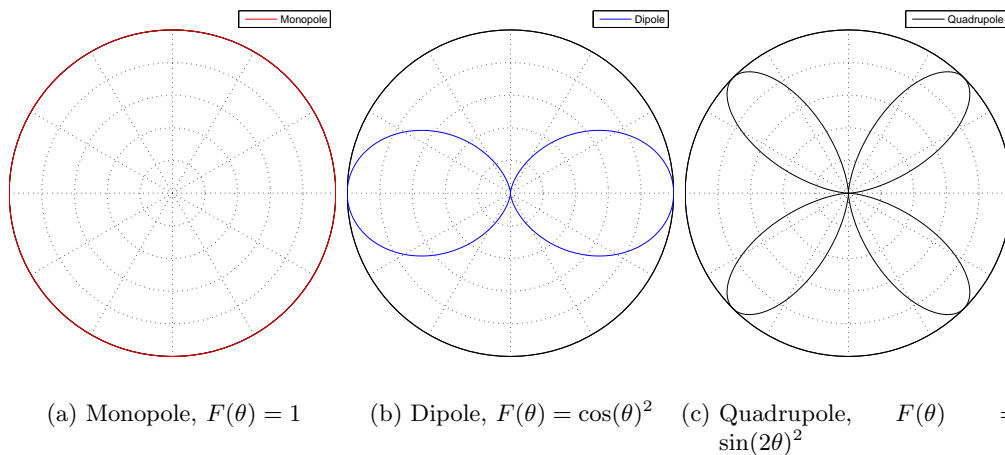


Figure 2.1: Directivity patterns of linear acoustic singularities; a) monopole, b) dipole, c) quadrupole

The far field acoustic intensity for those turbulent eddies that are concentrated at the vicinity of the half plane, leads to the following approximated scaling law for the acoustic

²The solution of any acoustic problem can be represented by a series singularities that fulfill the equations and can be superimposed linearly in order to create more complicated solutions. Similar to incompressible aerodynamics solutions, J.D. Anderson[4]

intensity, I , considering a series of simplifications on the theoretical approximation, [10];

$$I \approx \rho U^3 \left(\frac{U}{c_0} \right)^2 \frac{\delta}{R} \quad (2.1)$$

This flow velocity dependence on the fifth power represents an important approach of these theories, being δ a representative length scale of turbulent eddies passing by the trailing edge. This result provides the start-up for the semi-empirical formulations.

An interesting approach was introduced by M. Howe [35]. Lighthill's analogy was formulated using vorticity in order to outline the relation between vortex generation and in regards trailing edge noise. By applying this method, the acoustic analogy of Lighthill becomes modified in a way that sources are represented by turbulent vortices instead of the stress tensor mentioned before. And again, the formulation is built up of dipoles sources.

Parallel to these models, R.K. Amiet [2] proposed a theory for what is called turbulence inflow noise, being the noise radiated for a solid surface as a result of an incoming gust or unsteady flow. In this case, the region of noise radiation is not the trailing edge, but the leading edge. The model was developed for a linearised 3 dimensional flat plate, and it established the basis for most of the turbulence inflow noise models developed afterwards. However, the model of Amiet for inflow noise becomes more general, being able to re-express the formulation in order to be applied for a semi-infinite half plane with no leading edge and reproduce the previous formulations for trailing edge noise, i.e. FW-H [26]. In that sense, Amiet also established a formulation for trailing edge noise, [3].

Several corrections have been designed to better predict inflow turbulent noise along the frequency spectrum, being, M.V. Lowson [47], (see Section 2.2), the one to be outlined. He proposed a bypass correction for its empirical modelling in order to smooth the transition between low-frequency and high frequency inflow turbulence levels.

G. Guidati [34] develops a computational method based on Amiet's theory, combining it with a boundary element method in order to extract boundary layer properties considering airfoil geometry. Reasonable accuracy is achieved, however the extension of this inflow model is resumed up to 2D geometries and it becomes a time-consuming method when analysing different airfoils operating at different inflow conditions. P.J. Moriarty *et al.* [55], designed an empirical correction based on Guidati tests done on different airfoils, to include the airfoil geometry effect on Amiet's flat plate theory, and therefore, reduce computational time by losing accuracy.

Nevertheless, the influence of inflow noise coming from a wind turbine is somehow contradictory, although being an important source of noise for other rotary structure applications, such as computers fans or aircraft propellers, as V.P. Blandeau [15] shows when validating Amiet's model in different studies done at ISVR of Southampton University, it does not have the same expected effect on wind turbines.

There are still doubts whether it represents a source to be taken into account or not in wind turbines. Specially, as result of the terms required for the calculation, such as length scale eddy size. Studies performed at DTU-Risø show a certain disagreement on a NACA0015 [9]. Furthermore, trailing edge noise can often mask inflow noise, not observed in experimental tests (see Section 2.2), and occurring at high wind speeds where

can also be shadowed by background noise. Only a dedicated frequency analysis at low frequency might reveal this specific source of noise.

However, the introduction of enhanced modelling by V.P. Blandeau *et al.* [16] and J. Gill *et al.* [30] could provide more information about the behaviour of inflow noise.

2.2 Semi-empirical and Experimental Aeroacoustics

Several models based on previous research work done by J.E. Ffwoes-Williams *et al.* [26], and R.K. Amiet [2] were defined in order to predict high frequency noise, from both known sources; trailing-edge noise and inflow turbulent noise. To be outlined, the models defined by, F.W. Grosveld [33], W.B. De Wolf [24] (based on Grosveld formulations) and S.A.L. Glegg *et al.* [31] which included features to be used for wind turbine application (i.e. Blade Element momentum theory for the inflow parameters).

Nevertheless, significant results were achieved by measuring acoustic properties on wind tunnels equipped with an anechoic chamber. This kind of experiments started to be run during the 80s, surface pressure measurements done by T.F. Brooks *et al.* [21] preceded the most important results, also achieved by T.F. Brooks *et al.* [22] in the NASA Langley Research Center, as the main contribution to semi-empirical aeroacoustics.

By performing a series of aerodynamic and acoustic measurements on several 2D NACA0012 airfoils, they were able to define and distinguish different sources of trailing edge noise, fitting the scaling laws based on the results from J.E. Ffwoes-Williams *et al.* [26] and W.K. Blake [14] formulations. All the scaling laws were built on two parts; one that provides the absolute value, expressed in sound pressure level, and a second part that defines the spectral response. Tests were performed at different Reynolds numbers and Strouhal numbers in order to provide a wide range of data to fit scaling laws. One of the main features of this model is the dependence on boundary layer properties (see Chapter 3).

Although being a pure semi-empirical model, it has been used as a benchmark case for further applications. M.V. Lowson [47], improved the so called BPM model (standing for Brooks, Pope and Marcolini), and upgrading the simplified model for the inflow turbulence developed by R.K. Amiet [2] and creating a model for wind turbine application as previous authors did before. Lowson also established the distinction between semi-empirical models into several classes. From *Class I*, rule of a thumb models based on basic parameters such as rotor diameter or power, to *Class III*, where predictions are done using complete information about the operational behaviour of the wind turbine in regard the noise sources.

Since then, the BPM model have become the most significant semi-empirical results in wind turbine aeroacoustics, used in many occasions as a reference model for new Class III developments such as XNOISE [6], from the Institute of Aerodynamics and Gas Dynamics. This model is based on contributions from T.F. Brooks *et al.* [22], M.V. Lowson [47], and also F.W. Grosveld [33] coupled with a vortex-lattice method for the aerodynamic parameters. P. Fuglsang *et al.* [29] from Risø National Laboratory, used M.V. Lowson [47] model to develop and verify a code for wind turbine noise prediction based on semi-empirical formulations. They also established the basis for airfoil optimisation. Latter

improvements are NAFnoise by P.J. Moriarty *et al.* [54], from NREL or SILANT, by K. Boorsma *et al.* [17] from ECN, whose main difference is that both are coupled with X-FOIL [25] (originally from M. Drela) and R-FOIL,[18] respectively in order to assess the turbulent boundary layer properties for different airfoils.

Nevertheless, the uncertainties associated to measurements, [22], the strong dependence on the airfoil used (NACA0012), and the scale-up process and improved technology undergone by wind turbines, compromise the validity of the predictions. In that scenario, models such as the TNO model, initially proposed by R. Parchen [59] as a wrap-up model formulated from the previous theories shown in Section 2.1, started to be used as an alternative to the BPM model, appearing also in NAFnoise, [54], and under constant research improvement, [39] or [10]. Moreover, the evolution of computational numerical techniques applied to turbulent flows, such as RANS or LES methods, improves noticeable the results obtained regarding flow variables, despite of time-consuming operations in an attempt to improve accuracy when solving the different turbulent scales.

Parallel to all this modelling research effort, there has been a lot of wind tunnel testing and wind turbine testing (in field conditions), being the latter, the one that provides overall results although being in an uncontrolled atmosphere. The linear microphone array is a dedicated technique used to quantify and localise noise sources on a wind turbine. S. Oerlemans *et al.* [57] performed some field tests that pointed out the influence of directivity radiation effects of the noise sources localised on wind turbines. Figure 2.2a and Figure 2.2b clearly show that the main source of noise for a ground observer comes from the down stroke blade.

These tests also confirmed the influence of outer sections. Inflow velocities are higher, in comparison to inner sections, and therefore noise radiated can be neglected. However, all these tests revealed only trailing edge noise as a main source.

By quantifying noise sources using these field tests methodologies, it gave rise to design extra add-ons in order to reduce noise emissions. Within the European frame of R&D projects, the SIROCCO project³ was created by the Energy research Center of the Netherlands, [63], along with other partners such as the National Aerospace Laboratory, NRL, the Institute of Aerodynamics and Gas Dynamics of Stuttgart, IAG, and industry associates as General Electric GmbH, Composite Technology Center, CTC and Gamesa Eólica S.A. The aim of the tests was to reduce noise levels between 3dB to 6dB without reducing the aerodynamic performance.

Within this project frame, trailing edge serrations, initially proposed by M. Howe [36] as a mechanism to reduce the directivity efficiency of the trailing edge noise, were used. S. Oerlemans *et al.* [58] proved that serrated blades become quieter at low frequencies, while they are noisier at high frequencies as a result of a higher tip vortex. Nevertheless, an overall noise reduction, up to 3 dB, is achieved as wind speed increases without damaging the operational performance⁴.

³SIROCCO stands for Silent ROTors by aCoustiC Optimisation

⁴Slightly higher loads were detected in comparison to a baseline blade.



Figure 2.2: Localisation of noise sources. a) Gamesa 0.85 MW - 58.0, Zaragoza (ES), b) General Electric 2.3 MW - 94.0, Wieringermeer (NL), by courtesy of S. Oerlemans [57]

Intense experimental research on wind tunnel studies from IAG at University of Stuttgart, [48], [40], NREL, NRL [53] and DTU-Risø [11] have been going on during the last decade, in order to quantify and understand better the coupling effects between aerodynamics and acoustics with the recent improvements in wind tunnel measurement techniques. The quick introduction of PIV measurements, either planar or tomographic techniques done by Delft University of Technology, initiate a new era on wind tunnel measurements. A lot of research has been done in the last decade. Outline the work conducted by F. Scarano *et al.* [60], D. Ragni *et al.* [61] or V. Lorenzoni *et al.* [46] as example of relevant applications.

2.3 Computational Aeroacoustics methods, CAA

Direct Computational Acoustics is a numerical technique created in order to solve the sound radiation of a certain domain by capturing the pressure fluctuations without using the theoretical acoustic models introduced above these lines, and using instead, DNS or LES techniques to capture the high spread on temporal and spatial resolution involved. Although, being a similar field of study derived from the main CFD techniques, CAA shows up a series of challenges that makes these techniques to be much more expensive than common CFD.

Basically, the problem is based on solving fluctuations in pressure at a given location, and this raises some further problems. CFD techniques have evolved quite rapidly in

previous decades thanks to the intense research done and evolution of computers able to perform high number of calculations, however the problem is still the same; the higher the number of points in a fluid domain, the better the solution is approximated⁵, but at the same time, more computational time is required either to solve the vast amount of grid points for a steady state simulation or preserve the stability of a transient scheme, defined by the Courant number ($C = \Delta t U / \Delta x$). Therefore, there is always a trade-off between accuracy/cost when defining any numerical computation.

Nevertheless, high resolution is always required when using a direct computational aeroacoustic method, since it must be able to capture up to the small and quick pressure fluctuations generated by sound radiations. Moreover, the fact that turbulent flows are acoustic sound generators as commented before, increases the complexity, as result of the all the problems that turbulence modelling involves. Due to its random effects, including different scales and energy levels, it implies a clear tendency to used already known CFD techniques such as DNS or LES, making the computation a bit less expensive, for those cases or scenarios of industrial interest involving complex domains or critical conditions, specially, when applied into wind energy.

Another main difference between a CFD calculation and direct CAA methods is the flow domain. While the former can be restricted to those regions which are close a solid surface or possess substantial information about the behaviour of the flow, i.e. the wake of an airfoil, CAA implies considering the whole domain, as acoustic waves respond quickly and possess small intensities all the way towards the receiver path. Moreover, not only the receiver path must be considered, but also the effect of possible reflections from other directions, scattering and solid interactions. All these elements add complexity when designing the suitable domain to perform CAA calculations.

Regarding all these challenges, it seems there is a common practice towards CAA methods coupled with CFD codes equipped with turbulence model. However, as far as this technique has evolved, still shows a considerable loss in acoustic accuracy with respect to other techniques. This is reflected on calculations done by C. Tsai *et al.* [67] and J. Ask *et al.* [5], applied on other fields of acoustics. Even using expensive LES methods on cases for low Mach numbers, results are not satisfactory as initially expected as a consequence of the origin of formulation used, J. Larsson *et al.* [43].

Other concerns about CAA outlined in the literature by C. Tam [65], are the numerical noise resulting from the computational scheme used that can mask, in some cases, the pressure fluctuations that are, paradoxically, the objective of the CAA methods. Boundary conditions also provide a bunch of problems as a result of the vast range of materials that respond differently when interacting with noise, adding or absorbing acoustic energy, and therefore, modifying the pressure fluctuations field.

Detailed information about of CAA is out of the scope for this project, but summarising, challenges in CAA methods are the current state of the art regarding accurate prediction of solid surfaces within a turbulent stream. It is currently used for research purposes on airfoil optimisation and, applicable to industry up to some extent. Nevertheless, overall predictions of wind turbine noise are still out of scope of these methodologies in

⁵If it is a **consistent** method, a discrete method tends to the continuous solution as the grid space tends to zero, $\Delta x \rightarrow 0$. According to DTU course notes 41319 - Computational Fluid Dynamics

comparison with techniques less time-consuming with high reliable results although the uncertainties associated.

Aeroacoustics Modelling

This chapter becomes one of the most theoretical of the whole project as it introduces the theories behind aeroacoustics in order to get familiar with the main assumptions and hypothesis behind each model. Not all the models mentioned in Chapter 2 are deeply described. On the other hand, for the selected ones, there is mathematical content in order to ease the physical explanations.

The start-up of this chapter generalises on basic aeroacoustics theories but it tends progressively towards trailing edge noise and inflow turbulent noise as main wind turbine sources, historically described in the common applied aeroacoustics literature.

3.1 Lighthill Acoustic Analogy

M.J. Lighthill [44] established the basis of aeroacoustics theory as it has been mentioned in Chapter 2. In order to understand other models presented in the manuscript, it is interesting to show the basic hypotheses behind his analogy for an inhomogeneous and unbounded flow. Lighthill's analogy is derived from the well-known Navier-Stokes equations of mass and momentum conservation respectively;

$$\frac{\partial \rho}{\partial t} + \frac{\partial}{\partial x_i} \rho u_i = 0 \text{ for } i = 1, 2, 3 \quad (3.1)$$

$$\frac{\partial}{\partial t} \rho u_i + \frac{\partial}{\partial x_j} (\rho u_i u_j + p_{ij}) = 0 \text{ for } i, j = 1, 2, 3 \quad (3.2)$$

All the variables are a function of time and space, $\mathbf{f} = \mathbf{f}(t, x_i)$. Being ρ the flow density, u_i is the velocity vector and p_{ij} is the stress tensor for a Newtonian flow represented by;

$$p_{ij} = p \delta_{ij} - 2\mu e_{ij} = p \delta_{ij} - 2\mu \left[\frac{1}{2} \left(\frac{\partial u_i}{\partial x_j} + \frac{\partial u_j}{\partial x_i} \right) + \frac{2}{3} \frac{\partial u_k}{\partial x_k} \delta_{ij} \right] \quad (3.3)$$

By applying the time derivative to Eq.(3.1) and the divergence to Eq.(3.2) respectively;

$$\frac{\partial}{\partial t} \left[\frac{\partial \rho}{\partial t} + \frac{\partial}{\partial x_i} \rho u_i \right] = \frac{\partial^2 \rho}{\partial t^2} + \frac{\partial^2}{\partial t \partial x_i} \rho u_i = 0 \quad (3.4)$$

$$\frac{\partial}{\partial x_i} \left[\frac{\partial}{\partial t} \rho u_i + \frac{\partial}{\partial x_j} (\rho u_i u_j + p_{ij}) \right] = \frac{\partial^2}{\partial t \partial x_i} \rho u_i + \frac{\partial^2}{\partial x_i \partial x_j} (\rho u_i u_j + p_{ij}) = 0 \quad (3.5)$$

Subtracting Eq.(3.5) from Eq.(3.4);

$$\frac{\partial^2 \rho}{\partial t^2} - \frac{\partial^2}{\partial x_i \partial x_j} (\rho u_i u_j + p_{ij}) = 0 \quad (3.6)$$

The term $c_0 \partial^2 \rho / \partial x_i^2$ is subtracted from both sides of Eq.(3.6), being c_0 the speed of sound in equilibrium.

$$\frac{\partial^2 \rho}{\partial t^2} - c_0^2 \frac{\partial^2 \rho}{\partial x_i^2} = \frac{\partial^2}{\partial x_i \partial x_j} (\rho u_i u_j + p_{ij}) - c_0^2 \frac{\partial^2 \rho}{\partial x_i^2} \quad (3.7)$$

Previous Eq.(3.7) can be arranged by using the Kronecker delta, resulting into;

$$\frac{\partial^2 \rho}{\partial t^2} - c_0^2 \frac{\partial^2 \rho}{\partial x_i^2} = \frac{\partial^2}{\partial x_i \partial x_j} (\rho u_i u_j + p_{ij} - c_0^2 \delta_{ij}) \quad (3.8)$$

Where the term $\rho u_i u_j + p_{ij} - c_0^2 \delta_{ij}$ is the so called, Lighthills stress tensor. Thus, Lighthill analogy equation becomes;

$$\frac{\partial^2 \rho}{\partial t^2} - c_0^2 \frac{\partial^2 \rho}{\partial x_i^2} = \frac{\partial^2 T_{ij}}{\partial x_i \partial x_j} \quad (3.9)$$

Lighthill equations, Eqs.(3.1), (3.2) and (3.9) describe the motion of a wave moving at a speed of c_0 in a domain at rest as a result of external fluctuations introduced by the stress tensor. Lighthill stress tensor, T_{ij} , is the forcing term, being the mathematical modelling of sound generation. Effects of flow convection, shear stress and acoustic propagation constitute this term. In most of the cases, the meaningful term in Lighthill stress is convection, especially if Reynolds numbers are high enough.

The physical explanation behind Lighthill stress tensor is formulated on a force exerted by a distribution of quadrupoles bouncing stretching and squeezing each other in different configurations. Their instantaneous intensity per unit of volume is equal to the local stress.

Lighthill's analogy can be re-expressed using Kirchhoff equation in an adequate way, correcting functions with a retarded time¹, $t' = t - r_e/c_0$. By neglecting the near-field terms, the density fluctuations, for a given point within the domain, are given by the following expression;

$$4\pi c_0^4 (\rho(\mathbf{x}) - \rho_0) = \frac{(x_i - y_i)(x_j - y_j)}{|\mathbf{x} - \mathbf{y}|^3} \int_V \frac{\partial^2}{\partial t^2} T_{ij} \left[\mathbf{y}, t - \frac{|\mathbf{x} - \mathbf{y}|}{c_0} \right] \quad (3.10)$$

¹time delay between the source generation, \mathbf{x} and receiver, \mathbf{y}

3.2 Ffowcs, Hall and Hawkings Acoustic Analogy

After being introduced Lighthill's analogy in previous Section 3.1, it is interesting to have a look at the next significant result achieved in aeroacoustics theory. J.E. Ffowcs-Williams, L.H. Hall, [26] and D.L. Hawkings [27] extended Lighthill's formulation by applying the same analogy on a domain split in two parts; the surrounding flow and the moving surfaces. In that sense, this theory couples perfectly the acoustic radiation of an arbitrary moving surface within the flow in which is immersed. By means of this model, several applications can be analysed, such as helicopter wings, wind turbine blade, propellers, turbofans, etc. The complete derivation of this theory is not detailed here resulting in a complex mathematical proof. Nevertheless, it is interesting to analyse the final result. The FH-W model provides a similar wave equation with respect to Eq.(3.9);

$$\left(\frac{\partial^2}{\partial t^2} - c_0^2 \frac{\partial^2}{\partial x_i^2} \right) (\overline{\rho - \rho_0}) = \frac{\partial^2 \overline{T_{ij}}}{\partial x_i \partial x_j} - \frac{\partial}{\partial x_i} \left(p_{ij} \delta(f) \frac{\partial f}{\partial x_j} \right) + \frac{\partial}{\partial t} \left(\rho v_i \delta(f) \frac{\partial f}{\partial x_i} \right) \quad (3.11)$$

Observing Eq.(3.9), it can be seen that now, sound radiation is due to three sources instead of the one introduced by Lighthill's tensor in Eq.(3.9). Being $\overline{\rho - \rho_0}$ the density fluctuation. Eq.(3.11) turns into a similar expression as Eq.(3.10) by applying Kirchoff equation. The development is not relevant but the important aspect is that each source term has its following physical explanation;

- **1st Term:** Lighthill's stress tensor. Distribution of acoustic quadrupoles resulting from flow convection if Reynolds number is high enough. However, at low Mach numbers, it is not an efficient mechanism to radiate noise as it scales, basically, with the Mach number. The situation is completely different when considering an open jet flow, i.e. gas turbines, or turbofans.
- **2nd Term:** Distribution of acoustic dipoles over the solid surface. As an acoustic quadrupole is not efficient at low Mach numbers, at the proximities of a solid boundary, it turns into a most efficient mechanism; an acoustic dipole. N. Curle [23] first introduced this concept. The strength per unit of volume is equal to $p_{ij} n_j$.
- **3rd Term:** Distribution of acoustic monopole over the solid surface representing the perturbations introduced by the moving boundary. The instantaneous strength per unit of volume is ρv_i .

The distribution of dipoles is known as *Thickness Noise*, introduced by K.S. Brentner *et al.* [20], representing the displacement of a fluid as a result of a moving sound source. On the other hand, the distribution of monopoles is known as *Loading Noise* representing the force introduced on the fluid resulting from the acceleration of the moving surface.

The previous theory can be applied for multiple problems involving moving surfaces. However, when it is applied on airfoils, this one is modelled as a semi-infinite half scattering plate, being the trailing edge the discontinuity point between the surface and near wake flow that introduces noise radiation.

For those turbulent scales, mainly turbulent eddies, passing by close to the plate's trailing edge, the far field acoustic pressure can be simplified, according to [10], up to the following

expression;

$$p^2 \sim U^5 \frac{d\delta}{r_e^2} \sin^2 \left(\frac{\theta_e}{2} \right) \sin \Psi_e \cos^3 \gamma \quad (3.12)$$

Eq.(3.12) shows that noise intensity grows according to the fifth power of inflow velocity and being a function of turbulent length scale, δ^* . In previous Eq.(3.12), the directivity pattern of a semi-infinite plate along the chordwise direction, θ_e , and spanwise direction, Ψ_e , has been included. Since the scale of the turbulent eddies is considered smaller than the chordwise direction, the directivity pattern switches from low frequency dipole shape directivity to a more efficient directivity for high frequencies, pointing towards an imaginary leading edge. Figure 3.1 provides an idea of these two directivity functions.

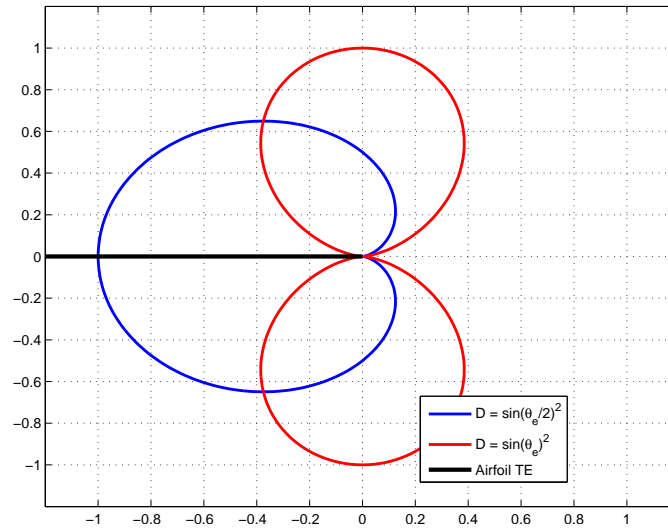


Figure 3.1: Trailing edge directivity patterns on a semi-infinite flat plate

As it can be seen from Figure 3.1, the radiation of trailing edge noise is emitted with a higher intensity towards the leading edge, and therefore, that is the main reason while wind turbine noise becomes more noticeable for a ground observer when listening to a down stroke blade passing by. Eq.(3.12) also shows a third angle dependency. This was introduced latter by M. Howe [36] when formulating the trailing edge serrations. Basically, this term affects the far field pressure by modifying the trailing edge exit angle. That is the fundamental concept behind a trailing edge serration; diminishing noise effectiveness, and so, intensity.

3.3 Turbulent Boundary Layer Trailing Edge Noise, TBL-TE

Having introduced the basics in aeroacoustics theory regarding noise emission from scattered plates interacting with a moving flow, it is time to introduce the main engineering and numerical models regarding aerodynamic noise, in particular, trailing edge noise, as one of the most important sources of noise in wind turbine applications.

Along this section, the most used models are introduced, analysed and described consistently. These are the well-known semi-empirical acoustic model BPM, T.F. Brooks *et al.* [22] and the Trailing Edge TNO model, R. Parchen *et al.* [59]. Both are presented in the coming sections along with the advantages and disadvantages of each formulation.

3.3.1 Trailing Edge Noise - BPM Model

Aerodynamic noise coming from the interaction between the solid trailing edge surface and a turbulent flow passing by, also known as airfoil self-noise, was thoroughly studied by T.F. Brooks *et al.* [22] testing NACA0012 airfoils inside a wind tunnel equipped with an anechoic chamber. The results were published in a NASA report called Airfoil Self-Noise and Prediction [22], which establishes the basis of a semi-empirical or engineering model in order to predict the different noise source that could occur due to such interaction already mentioned. This model is also known as BPM in honour to its developers: Brooks, Pope & Marcolini. According to their results obtained, the airfoil self-noise could be split into a series of trailing edge mechanisms:

- Turbulent boundary layer trailing edge noise (TBL - TE)
- Separation stall noise (TBL - SS)
- Tip vortex formation noise (TBL - TP)
- Laminar boundary layer vortex shedding noise (LBL - VS)
- Trailing edge bluntness vortex shedding noise (TEB - VS)

Each of the previous mechanisms could coexist with the others or it would only occurred under specific flow conditions such as stall conditions.

T.F. Brooks *et al.* [22] established sound pressure level expressions, SPL, for each of the mechanisms, based on the scaling laws from the existing aeroacoustic theory, J.E. Ffowcs-Williams *et al.* [26]. The resulting expressions consist of different terms. The first term takes into account geometric and aerodynamic parameters providing a scaling law for the overall level, while the second one defines the spectrum within a typical range from 20 Hz to 20 kHz.

In the coming sections below, the aerodynamic mechanisms belonging to airfoil self-noise are analysed and described thoroughly along with their relative importance. The semi-empirical equations that describe the relation between inflow conditions and sound pressure level are also displayed.

Turbulent Boundary Layer Trailing Edge Noise (TBL-TE)

The turbulent boundary layer trailing edge noise is a broadband noise source originated when a turbulent boundary layer attached to the blade passes by the trailing edge before being shed into the wake. Turbulence originates pressure fluctuations around the discontinuity introduced by the trailing edge, in both, suction and pressure sides of the airfoil.

In this case, the noise mechanism consists of a series of non-stationary structures, mainly vortices, which appear inside the turbulent flow in the boundary layer. The interaction of such vortices with the discontinuity introduced in the solid surface by the airfoil trailing edge originates this source of noise, as pressure fluctuations exist within such structures. Figure 3.2 gives an idea of such an effect.

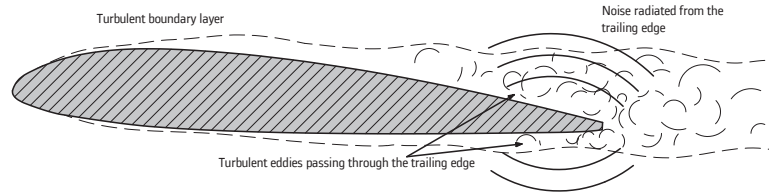


Figure 3.2: Sketch of turbulent boundary layer trailing edge noise, TBL-TE

Given a Reynolds number and an angle of attack, the turbulent boundary layer occurs at a certain position. If AoA is low, the flow separation of this turbulent boundary layer appears near the trailing edge. Each side of the airfoil with a well-developed boundary layer produces TBL - TE noise independently of the other side. Therefore, the amount of noise generated may account for these two contributions plus an AoA terms, since tests were done over a symmetric airfoil, NACA0012, thus, a third term AoA-dependent was introduced to account for extra effects such as non-zero lift. The sum of these three sources originates the so called turbulent boundary layer trailing edge noise;

$$\text{SPL}_{\text{TBL-TE}} [\text{dB}] = 10 \log_{10} \left(10^{\text{SPL}_p/10} + 10^{\text{SPL}_s/10} + 10^{\text{SPL}_\alpha/10} \right) \text{ if } \alpha < 12.5^\circ \quad (3.13)$$

Turbulent boundary layer trailing edge noise is considered to be the main source of aerodynamic noise, except when the airfoil is in stall conditions as details Section 3.3.1. As mentioned before, this source is a broadband noise normally expected between $700 [\text{Hz}] < f < 2 [\text{kHz}]$ and the noise source become meaningful at the outer sections of a wind turbine as S. Oerlemans *et al.* [57] experienced on field testing.

The TBL - TE noise prediction model follows, partially, the scaling law derived from far field pressure spectrum first formulated by J.E. Ffowcs-Williams *et al.* [26] regarding a turbulent boundary layer passing by a scattering half plate. According to T.F. Brooks *et al.* [22], the dependence on the fifth power of Mach number comes from simplifications on the FW-H equation. The rest of parameters are fit accordingly the results obtained when testing the NACA0012.

The BPM model is also normalized using the main boundary layer scales such as boundary layer thickness δ , BL displacement thickness δ^* , and BL momentum thickness θ . So, the expression is split into scaling terms and spectrum terms;

$$\text{SPL} [\text{dB}] = 10 \log_{10} \left(M^5 \frac{\delta d}{r_e^2} \right) + F(\text{St}) + K \quad (3.14)$$

Where, $F(\text{St})$ defines the noise spectrum shape based on a Strouhal number [dB]. Basically, $F(\text{St})$ contains the information of the SPL at each frequency of the spectrum. Finally, K is the scaled level corresponding to the peak locations of the Strouhal number inside the spectrum [dB].

Eq.(3.14) is the generic form of the BPM source model, however, several experiments carried out by T.F. Brooks *et al.* [22] show that the normalized data is highly affected by the Reynolds and Mach number as well as the angle of attack. Therefore, it is possible to express both, the SPL expressions spectral shape and the scale level as a function of these parameters.

In particular, for the case of turbulent boundary layer trailing edge noise, the SPL expressions for pressure side, suction side and separation flow are;

$$\text{SPL}_p [\text{dB}] = 10 \log_{10} \left(\frac{\delta_p^* M^5 d\bar{D}_H}{r_e^2} \right) + \mathbf{A} \left(\frac{\text{St}_p}{\text{St}_1} \right) + (K_1 - 3) + \Delta K_1 \quad (3.15)$$

$$\text{SPL}_s [\text{dB}] = 10 \log_{10} \left(\frac{\delta_s^* M^5 d\bar{D}_H}{r_e^2} \right) + \mathbf{A} \left(\frac{\text{St}_s}{\text{St}_1} \right) + (K_1 - 3) \quad (3.16)$$

$$\text{SPL}_\alpha [\text{dB}] = 10 \log_{10} \left(\frac{\delta_s^* M^5 d\bar{D}_H}{r_e^2} \right) + \mathbf{B} \left(\frac{\text{St}_s}{\text{St}_2} \right) + K_2 \quad (3.17)$$

Where, δ_p^* and δ_s^* are the pressure and suction side boundary layer displacement thickness respectively, A and B are spectrum shapes as a function of Strouhal number, St, based on δ_p^* and δ_s^* as well as other parameters such as Reynolds number Mach number and AoA . Finally, K_1 , K_2 and ΔK_1 are scaled values.

All these terms are deeply described in Appendix B B. Finally, the total contribution to TBL - TE is obtained by applying Eq.(3.13)

Turbulent Boundary Layer - Separation Stall Noise (TBL-SS)

The separation stall noise mechanism is based on the high pressure fluctuations occurring when the flow is no longer attached to the airfoil as a result of a high angle of attack. The size of the turbulent boundary layer on the suction side becomes wider, forming large scale eddies (unsteady structures) whose interactions with the upper surface of the airfoil introduce pressure fluctuations at lower frequency. Usually, the larger the scale of the turbulent eddies, the lower is the frequency of wake shedding. Figure 3.3 shows a representation of separation stall noise.

When the airfoil is close to stall, noise can be increased by more than 10 [dB] relative to turbulent boundary layer trailing edge noise (as mentioned previously, main source of aerodynamic noise at low angles of attack). Beyond limiting angles, deep stall noise would be the only major contributing source radiating a low frequency noise.

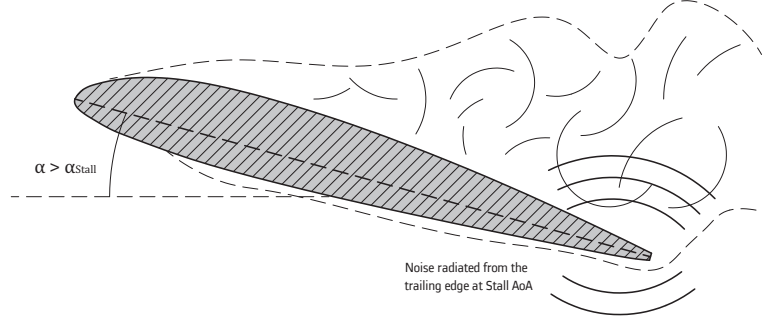


Figure 3.3: Sketch of turbulent boundary layer separation stall noise, TBL-SS

For the separation stall noise, a similar expression to Eq.(3.14) can be obtained, but several corrections have to be applied in order to reproduce the effects occurring during tests. Thus, the sound pressure level can be expressed as;

$$\text{SPL}_p [\text{dB}] = -\infty \quad (3.18)$$

$$\text{SPL}_s [\text{dB}] = -\infty \quad (3.19)$$

$$\text{SPL}_\alpha [\text{dB}] = 10 \log_{10} \left(\frac{\delta_s^* M^5 d \overline{D}_L}{r_e^2} \right) + \mathbf{A} \left(\frac{\text{St}_s}{\text{St}_2} \right) + K_2 \quad (3.20)$$

In this case, it is suitable to take, as scale length, the boundary layer displacement thickness of the suction side, δ_s^* , because it is representative of the flow situation, but this thickness must be calculated for the stall operation as a result of the boundary layer detachment from the upper surface.

With respect to the spectral shape, B is replaced by A. Then, the contributions of SPL_p and SPL_s can be neglected.

$$\text{SPL}_{\text{TBL-SS}}[\text{dB}] = 10 \log_{10} \left(\underbrace{10^{\text{SPL}_p/10}}_{=0} + \underbrace{10^{\text{SPL}_s/10}}_{=0} + 10^{\text{SPL}_\alpha/10} \right) \quad (3.21)$$

Turbulent Boundary Layer - Tip Vortex Noise (TBL-TV)

The tip noise has been identified with the turbulence generated by the tips vortices at the blade tip region where the high pressure side (lower surface) contacts with the low pressure side (upper surface). The pressure gradient between the lower and upper surfaces rises to a rotational flow over the airfoil which mostly contains a vortex with a thick viscous turbulent core.

The mechanism for tip noise generation turns out to be trailing edge noise due to the passage of the flow turbulence over the trailing edge at the tip region. This phenomenon is equivalent to the turbulent boundary layer trailing edge, according to T.F. Brooks *et al.* [22], but with a clear 3D nature as Figure 3.4 intends to represent. In terms of relative importance, this source contribution is less than the ones introduced previously, or it could be seen as a particular case of TBL-TE. However, it can introduce considerable amounts of noise at higher broadband frequencies.

Blade's tip geometry influences drastically on the noise intensity as well as the local angle of attack. An accurate tip design, such current state-of-art winglets, along with a reverse twist, could imply reduction of tip noise.

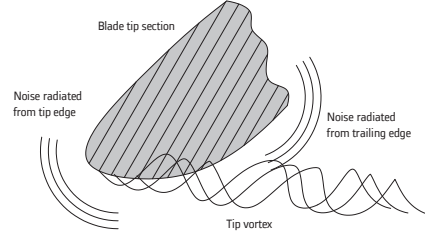


Figure 3.4: Sketch of Turbulent boundary layer - tip vortex formation noise, TBL-TV

The scaling law for tip vortex noise follows the tendency of the previous models, but with some particularities. The SPL expression is;

$$\text{SPL}_{\text{TBL-TP}}[\text{dB}] = 10 \log_{10} \left(\frac{M^5 (1 + 0.036\alpha_{\text{tip}})^3 l^2 \overline{D_H}}{r_e^2} \right) + \mathbf{C}(\text{St}'') \quad (3.22)$$

The angle of attack that appears on Eq.(3.22) represents the angle of attack of the tip region. Regarding the Strouhal number, it is built on the following basis;

$$\text{St}'' = \frac{fl}{U_{\text{max}}} = \frac{fl}{U(1 + 0.036\alpha_{\text{tip}})} \quad (3.23)$$

Furthermore, the scale length chosen, l , represents the span wise extent at the trailing edge as a result of the detachment of a vortex with a Γ strength as shows Figure 3.5.

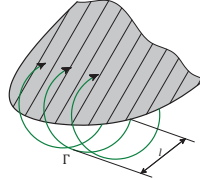


Figure 3.5: Sketch of the span wise extension at the tip region

The span wise extent at the trailing edge can be assessed using the following expressions for rounded tips and flat tips respectively;

$$\frac{l}{c} = 0.008\alpha_{\text{tip}} \quad (3.24)$$

$$\frac{l}{c} = \begin{cases} 0.0230 + 0.0169\alpha_{\text{tip}} & 0^\circ \leq \alpha_{\text{tip}} \leq 2^\circ \\ 0.0378 + 0.0095\alpha_{\text{tip}} & \alpha_{\text{tip}} > 2^\circ \end{cases} \quad (3.25)$$

Nevertheless, the latter expression for flat tips has not been validated experimentally. The AoAs appearing on Eqs.(3.22) and (3.24) are slightly different to the expected AoA at tip, since it is corrected by the loading effects that can differ from a reference case with no loads applied. Therefore, the corresponding lift curve must be as known to assess the correct angle of attack.

Laminar Boundary Layer Vortex Shedding (LBL-VS)

Vortex shedding occurs when laminar boundary layer exists over the entire surface of an airfoil, typically, at inner sections of the rotor span where Reynolds numbers are lower than outer sections ($Re \approx 10^5$) and laminar boundary layers are fully developed. The source mechanism turns out to be the interaction between the instabilities of the LBL in the transition region with the vortices shed in the wake passing by the trailing edge. Those produce pressure fluctuations.

The vortex shedding is coupled to excited aerodynamic feedback loops. Those take place between the airfoil trailing edge and an upstream source point on the surface where instability waves, known as Tollmien-Schlichting waves² [32], originate inside the LBL.

The resulting noise spectrum is composed of quasi-tones related to the shedding rates at the trailing edge and radiated at high frequencies from the blade surface. The effect becomes more important in the pressure side of the airfoil. Nevertheless, laminar boundary layers are not so common in conventional wind turbines, specially, because laminar layers are rarely found in wind turbine applications, hence, this source of self-noise is not contemplated in any of the studies found in common literature.

There are no laminar boundary layer vortex shedding noise scaling methods established in the literature because of the erratic behaviour of the multiple tones in the narrow band spectra and the general complexity of the mechanism. However, two key results from experimental tests [22] provide a scaling guidance:

- The gross trend of the frequency dependence is found to scale on a Strouhal basis with the relevant length scale being the boundary layer thickness on the pressure side δ_p .
- Overall sound levels tend to coalesce to a unique function of Reynolds number when SPL is normalized in the fashion of TBL - TE noise.

The scaling approach is then similar; consisting of a universal spectral shape with Strouhal dependence plus sound level terms modelled as a function of boundary layer parameters and as well as Reynolds and Mach number. Therefore, the SPL expression is;

$$\text{SPL}_{\text{LBL-VS}} [\text{dB}] = 10 \log_{10} \left(\frac{\delta_p M^5 d \bar{D}_H}{r_e^2} \right) + \mathbf{G}_1 \left(\frac{\text{St}'}{\text{St}'_{\text{peak}}} \right) + \mathbf{G}_2 \left(\frac{\text{Re}_c}{(\text{Re}_c)_0} \right) + \mathbf{G}_3(\alpha) \quad (3.26)$$

Where, \mathbf{G}_1 defines the spectrum shape in terms of the ratio between Strouhal number based on δ_p and its peak value. \mathbf{G}_2 specifies the peak scaled level shape curve as a function of Reynolds number. Finally, \mathbf{G}_3 introduces the angle dependent level for the shape curve of \mathbf{G}_2 . All these functions are described in Appendix B.

Trailing Edge Bluntness Vortex Shedding Noise (TEB-VS)

Noise due to vortex shedding from blunt trailing edge was first established by T.F. Brooks *et al.* [21], to be an important airfoil self-noise source.

²T-S wave is a stream wise instability which arises in a viscous boundary layer. It one of the most common mechanisms by which a laminar boundary layer becomes turbulent.

Trailing edge bluntness noise is produced as a result of the abrupt ending of the trailing edge. There is an interaction of the vortices shed into the wake at specific rates and the boundary layer passing through the trailing edge that radiates noise. Typically, it is originated on those airfoils with blunt trailing edges where Von Karman vortices can easily appear. In fact, the effect is similar to the Von Karman's street for a flow passing a cylinder, [64], approximately between $4 < Re < 400$) as clearly shows Figure 3.6. These vortices are characterized by pressure fluctuations occurring at specific frequencies, and therefore, radiating noise on a tonal basis.

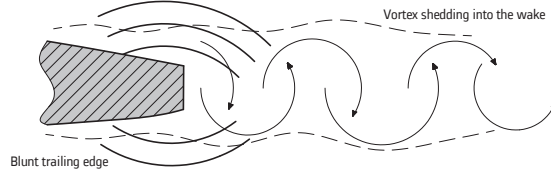


Figure 3.6: Sketch of trailing edge bluntness vortex shedding noise, TEB-VS

Trailing edge bluntness noise becomes important when the bluntness length is the same order of magnitude as the boundary layer thickness at the trailing edge region, so the airfoil trailing edge's geometry modifies noise intensity.

Nevertheless, trailing edge bluntness vortex shedding noise is far to occur regarding new blades designs. Trailing edge thicknesses, from outer sections, are accurately treated to avoid blunt edges. Moreover, the appearance of tones on a narrow band can be masked by the presence of trailing edge noise along the blade. Although there are scaling laws proposed by T.F. Brooks *et al.* [22], it is difficult to reproduce as a result of a strong dependence on inflow conditions which can make the phenomenon occur or not. Recent studies show that if the trailing edge thickness is small enough, there is a high probability that it does not radiate noise; otherwise, this source should be included.

Based on the scaling approach taken for the turbulent boundary layer trailing edge noise (TBL - TE) and the laminar boundary layer vortex shedding noise (TEB - VS), the sound level, frequency and spectral shape are modelled as functions of inflow conditions and trailing edge geometric parameters.

As mentioned before, trailing edge bluntness vortex shedding noise becomes relevant when the ratio between trailing edge thickness and boundary layer displacement thickness is; $h/\delta^* \geq 1$. Then the contribution of TEB-VS has a broader spectrum centred in the high frequency region ≥ 1 kHz, while is less important for lower ratio according to W.K. Blake [14] and T.F. Brooks *et al.* [22].

The trailing edge bluntness noise scaling law given in sound pressure level is predicted by;

$$\text{SPL}_{\text{TEB-VS}} [\text{dB}] = 10 \log_{10} \left(\frac{hM^{5.5}d\bar{D}_H}{r_e^2} \right) + \mathbf{G}_4 \left(\frac{h}{\delta_{\text{avg}}^*}, \Psi \right) + \mathbf{G}_5 \left(\frac{h}{\delta_{\text{avg}}^*}, \Psi, \frac{St'''}{St_{\text{peak}}'''} \right) \quad (3.27)$$

Compared to the other scaling laws, a 5.5 power for Mach dependence in the sound level was experimentally determined to give a better fitting than either a 5 or 6 power, [22].

\mathbf{G}_4 function determines the peak level of the spectrum curve [dB], meanwhile \mathbf{G}_5 introduces the shape of the spectrum (see Eq.(3.27) the Strouhal ratio dependence). Both

functions depend on two geometric parameters: the ratio h/δ_{avg}^* called degree of bluntness where;

$$\delta_{\text{avg}}^* = \frac{\delta_p^* + \delta_s^*}{2} \quad (3.28)$$

The other parameter, Ψ , represents the trailing edge solid angle. \mathbf{G}_5 expressions are fitted with $\Psi = 0^\circ$ and $\Psi = 14^\circ$ solid angles belonging to the flat plate of NACA 0012 airfoil tested in [22] respectively. Intermediate values must be interpolated. Detailed information about \mathbf{G}_4 and \mathbf{G}_5 scaling functions is found in Appendix B.

3.3.2 Trailing Edge Noise - TNO Model

A more analytical model regarding trailing edge noise radiated on a turbulent boundary layer was formulated by R. Parchen [59]. The model itself is derived from a combination of FH-W model introduced in Section 3.2, combined with the results of diffraction theory over a flat plate from N. Curle [23] and also contributions from the vortex analogy developed by M. Howe [35]. The resulting formulation provides an expression for pressure fluctuations spectrum;

$$\mathbf{P}(k_1, k_3, \omega) = 4\rho^2 \left(\frac{k_1^2}{k_1^2 + k_3^2} \right) \int_0^\infty \Lambda_2(x_2) \cdot \left(\frac{dU_1(x_2)}{dx_2} \right)^2 \cdot \Phi_{22}(\mathbf{k}, \omega) \cdot \overline{u_2^2} \cdot \Phi_m(\omega - k_1 U_c) e^{-2|\mathbf{k}|x_2} dx_2 \quad (3.29)$$

From the previous integral equation, \mathbf{k} is the wave number vector defined in a orthogonal space of (k_1, k_2, k_3) , Λ_2 is the vertical turbulence length scale which provides an estimation of the eddies size, $\overline{u_2^2}$, is the RMS of vertical velocity fluctuations, being one of the Reynolds stress terms. Φ_{22} represents the vertical velocity fluctuations spectrum and, Φ_m is the moving axis spectrum which defines the change on Φ_{22} as a result of the generation and destruction of eddies during the convection over the trailing edge, at a convection speed of U_c . Finally, U_1 is the streamwise mean velocity, aligned with the x-direction whose gradient along the vertical direction, x_2 , is associated to wall shearing. Figure 3.7 shows a rough visual explanation of how TNO model is formulated.

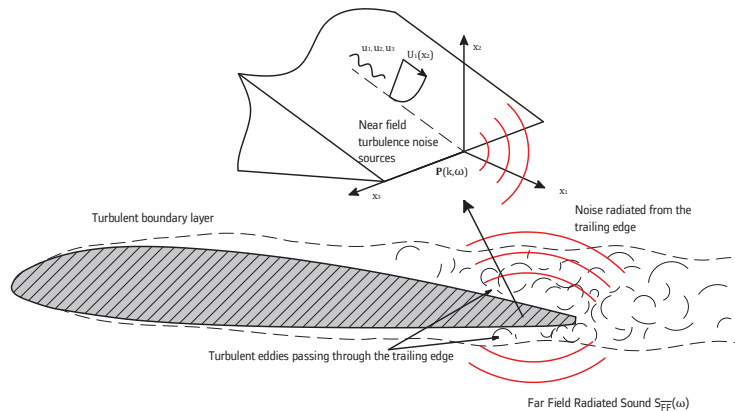


Figure 3.7: Trailing edge noise mechanism based on TNO model. Sketch based on M. Kamruzzaman [39] research work

From Figure 3.7 it can be visualised the process already mentioned when introducing BPM model in Section 3.3.1; the fluctuations originated within a turbulent boundary layer introduce pressure fluctuations at the vicinity of a sharp edge, implying a radiation of sound towards a far field position. It is in the core of the boundary layer and surface geometry the mystery of how noise is radiated in a specific way or another.

The initial TNO model is based on a kinetic energy spectrum for isotropic turbulence, specifically, the Von Karman three-dimensional spectrum;

$$E(k) = \frac{110\Gamma(5/6)}{27\sqrt{\pi}\Gamma(1/3)} \frac{k_T}{k_e} \frac{(k/k_e)^4}{[1 + (k/k_e)^2]^{17/6}} \quad (3.30)$$

From Eq.(3.30), k_e is the wave number of energy-containing eddies³, and k_T represents the turbulence kinetic energy;

$$k_T = \frac{1}{2}(\overline{u_1^2} + \overline{u_2^2} + \overline{u_3^2}) \quad (3.31)$$

Considering a case of isotropic turbulence, Eq.(3.31) becomes $k_T = 3/2\overline{u_2^2}$. M. Kamruzzaman [39] provides a research study on the effects of using anisotropic turbulence model on the sound radiation, obtaining better results, in general than using a simple isotropic model. Nevertheless, isotropic turbulence is going to be considered along this report as a result of the complexity involved in the modelling it.

$$\Phi_{22}(k_1, k_3) = \frac{4}{9\pi k_e^2} \frac{(k_1/k_e)^2 + (k_3/k_e)^2}{[1 + (k_1/k_e)^2 + (k_3/k_e)^2]^{7/3}} \quad (3.32)$$

Finally the moving spectrum, Φ_m is usually defined as a Gaussian spectrum with the following form;

$$\Phi_m(\omega - U_c k_1) = \frac{1}{\alpha_{\text{Gauss}} \sqrt{\pi}} e^{-[(\omega - U_c k_1)/\alpha_{\text{Gauss}}]^2} \quad (3.33)$$

This Gaussian constant, α_{Gauss} is defined as a function of the eddy convection velocity, U_c which at the same time can be described by the boundary layer mean streamwise velocity, U_1 .

$$\alpha_{\text{Gauss}} = 0.05 \frac{c_\alpha U_1(x_2)}{\Lambda_2} \quad c_\alpha = 0.09 \quad (3.34)$$

The relation between pressure fluctuations near the trailing edge surface described by Eq.(3.29), and the radiated far field spectrum, \mathbf{S}_{FF} , at a given receiver location r_e , is derived from M. Howe [35] results, without considering amplitude modulation or Doppler effects. Therefore, the expression for one side surface becomes;

$$\mathbf{S}_{FF}(\omega) = \frac{d}{4\pi r_e^2} \sin\left(\frac{\theta_e}{2}\right) \sin \Psi_e \int_{-\infty}^{\infty} \frac{\omega}{c_0 k_1} \mathbf{P}(k_1, 0, \omega) dk_1 \quad (3.35)$$

The same directivity pattern can be observed again, previously introduced in Section 3.3.2. This formulation provided good agreements when compared to pressure measurements carried out by T.F. Brooks *et al.* [21] on airfoils in wind tunnel tests. The validity of the previous approach is limited within a frequency range which the airfoil can be considered

³ $\Gamma(x)$ is the so-called Gamma function, mathematically defined as $\Gamma(x) = \int_0^\infty t^{x-1} \exp -tdt$

as non-compact, this means that the wavelength of turbulent scale must be smaller than the local chord.

$$\lambda \ll c$$

The question now is how all the term from Eq.(3.29) can be modelled when assuming isotropic turbulence conditions, since most of them depend on the boundary layer characteristics. In the current state-of-art, there are a couple of models approximating the previous terms, the first one is based on an integral boundary layer model, while the other one, it is based on RANS CFD methods considering the advances in such as technique.

TNO Modelling Based on an Integral Boundary Layer Method

The first approach of modelling all the terms already introduced for the surface pressure fluctuations in Eq.(3.29) is, basically, applying an integral boundary layer method. This methodology consists of solving a potential flow around a given surface by means of inviscid equations of motion. Then, using the pressure field obtained, the boundary layer is accordingly scaled whose presence was not initially considered. Therefore, the process becomes iterative until it converges.

A reader, familiarised in computational fluid mechanics, recognises easily this method as being the one used in the so famous X-FOIL software for airfoil design developed by M. Drela [25]. From that approach, multiple variables of interest can be assessed, i.e. skin friction coefficient, C_f , the boundary layer thickness, δ , boundary layer displacement thickness, δ^* , and boundary layer momentum thickness, θ^* .

Once all this information is possessed, it is possible to estimate the boundary layer properties, necessary for the TNO model. Starting from the vertical velocity gradient, Cole's law is used for determining the velocity profile, which combines the law of the wall scaled with $y^+ = u^*x_2/\nu$ and the law of the wake, scaled with x_2/δ . Combining both of them, they become;

$$U_1(x_2) = u^* \left(\frac{1}{\kappa} \log \left(\frac{u^*x_2}{\nu} \right) + B + \frac{1}{2}W \left(\frac{U_e}{u^*} - \frac{1}{\kappa} \log \left(\frac{u^*x_2}{\nu} \right) - B \right) \right) \quad (3.36)$$

where $\kappa = 0.41$ is the Von Karman constant, $B = 5.5$ and $u^* = U_e\sqrt{C_f/2}$ is the friction velocity, being, C_f , the skin friction coefficient. From Eq.(3.36) the wake function, W , can be define as;

$$W = 1 - \cos \left(\frac{\pi y_2}{\delta} \right) \quad (3.37)$$

By deriving Eq.(3.36), with respect to the vertical direction, represented by, x_2 , the derivative term from Eq.(3.29) can be easily calculated.

The next term is the turbulence length scale Λ_2 . The approach for defining this term is based on the turbulence mixing length, l_m , initially proposed by H. Schlichting and provided by F. Bertagnolio [10] as;

$$l_m = 0.085\delta \tanh \left(\frac{\kappa x_2}{0.085\delta} \right) \quad (3.38)$$

Then, the integral length scale can be approximated by

$$\Lambda_2 = l_m/\kappa \quad (3.39)$$

Considering a case for isotropic turbulence, the turbulence length scale can be used to estimate k_e by means of the following expression;

$$\Lambda_2 = \frac{\sqrt{\pi}\Gamma(5/6)}{\Gamma(1/3)} \frac{1}{k_e} \quad (3.40)$$

Therefore, the wave number of energy containing eddies is roughly $k_e \approx 0.7468/\Lambda_2$, which is necessary in order to assess the vertical velocity fluctuations spectrum, Φ_{22} , by means of Eq.(3.32).

The remaining quantity is the vertical velocity fluctuations, $\overline{u_2^2}$ which are calculated by means of the turbulent kinetic energy, k_T . This quantity is assessed using the hypothesis of turbulent viscosity or turbulent dissipation, ν_t , relating this quantity to the mixing length.

$$k_T = \sqrt{\frac{\nu_t}{C_\mu} \left(\frac{dU_1(x_2)}{dx_2} \right)^2} \quad \text{where } \nu_t = l_m^2 \left| \frac{dU_1(x_2)}{dx_2} \right| \quad (3.41)$$

where $C_\mu = 0.09$. Finally, the vertical velocity fluctuations are assumed to be proportional to the turbulent kinetic energy;

$$\overline{u_2^2} = \alpha_u k_T \quad (3.42)$$

Being $\alpha_u = 0.45$ for airfoil suction side, and $\alpha_u = 0.30$ for the pressure side respectively. Therefore, by calculating all these quantities as a function of the inflow conditions, it is possible to estimate the far field pressure field radiated by an airfoil.

TNO Modelling Based on RANS Techniques

By scanning carefully some of the expressions introduced along Section 3.3.2, the reader could easily realise one of the main drawbacks of the previous modelling. When flow separation occurs, the skin friction coefficient becomes automatically 0 or negative. Eq.(3.36) cannot handle such behaviour as a result of how it was formulated⁴. The solution to this problem can be found by using current CFD techniques, in which most of the previously mentioned quantities are already a direct output of a CFD calculation.

By using the appropriate meshing over the region of interest, the boundary layer shear, $\partial U_1(x_2)/\partial x_2$, velocity vertical fluctuations, $\overline{u_2^2}$ and turbulent kinetic energy, k_T , can be easily obtained. Only the turbulence length scale remains unknown, even using a numerical technique. Studies performed at IAG by L. Lutz *et al.* [48] and [41], from Stuttgart University, confirms the relevance of this parameters on noise generation.

For an isotropic turbulence analysis, the length scale is recalled from previous Section 3.3.2 as;

$$\Lambda_2 = \frac{\sqrt{\pi}\Gamma(5/6)}{\Gamma(1/3)} \frac{1}{k_e} \quad (3.43)$$

Instead of using the mixing length scale, l_m , in this case, the asymptotic behaviour of the vertical velocity fluctuations spectrum is compared with the well-known asymptotic

⁴The square root or the logarithm penalises it

trend of the Kolmogorov spectrum in the inertial sub-range. The wavenumber can vary from $1/l \ll \kappa \ll 1/\eta$ ⁵. The Kolmogorov Spectrum within this range is defined as;

$$E(k) = C \frac{\varepsilon^{2/3}}{k^{5/3}} \quad (3.44)$$

Being C and empirical constant approximately equal to 1.5. By considering $k \rightarrow \infty$ in both Eqs.(3.30) and (3.44) and comparing the asymptotic behaviour between the Von Karman and Kolmogorov spectra, an approximation for the wavenumber of energy containing eddies can be obtained;

$$\begin{aligned} E_{\text{Karman}}(k)|_{k \rightarrow \infty} &= E_{\text{Kolmogorov}}(k)|_{k \rightarrow \infty} \\ \frac{110\Gamma(5/6)}{27\sqrt{\pi}\Gamma(1/3)} k_T k_e^{2/3} &= C \varepsilon^{2/3} \\ k_e &= \left(\frac{27\sqrt{\pi}\Gamma(1/3)C}{110\Gamma(5/6)} \right)^{3/2} \frac{\varepsilon}{k_T^{3/2}} \\ k_e &= 1.9274 \frac{\varepsilon}{k_T^{5/3}} \end{aligned} \quad (3.45)$$

and therefore, combining the previous result with Eq.(3.43) it provides an approximation to estimate the length scale as;

$$\Lambda_2 = 0.387 \frac{k_T^{3/2}}{\varepsilon} \quad (3.46)$$

This approach can be used by using a RANS CFD model to solve the flow field coupled with a $k - \varepsilon$ or $k - \omega$ SST model to close the numerical problem. By solving these variables within the boundary layer, all the required properties for the TNO model can be assessed, even including the latest approximation for the turbulent length scale, Λ_2 , using Eq.(3.46).

Nevertheless, the previous developments here exposed have been based on assuming isotropic turbulence. Despite that, the TNO model, based under these assumptions, always underestimates acoustic measurements as M. Kamruzzaman *et al.* [40] shows in their validation analysis. Regarding that, turbulence nature is a completely random process so that, it is a conservative approach using isotropic turbulence. The degree of anisotropy between two different flow components could be approximated by;

$$\frac{\overline{u_i^2}}{\overline{u_j^2}} = \beta_{ij}$$

Therefore, there has been a lot of effort and research during the last few years to tune and improve the formulation given by the TNO-Blake model in order to diminish the uncertainty between measurements and predictions. It must be outlined contributions done by IAG at Stuttgart University and DTU-Risø in Denmark trying to improve the formulation by adding turbulence anisotropy effects. An example of it, M.Kamruzzaman *et al.* [39] and [40], introduced turbulence anisotropy on the vertical velocity spectrum formulation, Eq.(3.32), whose validation was done on a NACA0012. Similar what has

⁵Being η the Kolmogorov micro-scale

been done recently by F. Bertagnolio *et al.* [9] over a NACA0015, providing an equivalent expression for the vertical velocity spectrum formulation.

$$\Phi_{22}(k_1, k_3, k_e, \beta_{1,3}) = \frac{4}{9\pi k_e^2} \beta_1 \beta_3 \frac{(\beta_1 k_1/k_e)^2 + (\beta_3 k_3/k_e)^2}{[1 + (\beta_1 k_1/k_e)^2 + (\beta_3 k_3/k_e)^2]^{7/3}} \quad (3.47)$$

Being β_1 and β_3 the stretching factors defining the degree of anisotropy. Besides anisotropy, these studies also revealed the necessity of introducing a multiplicative factor of 2 when evaluating the vertical integral scale length, γ_2 in order to be consistent with the given definition of correlation length, and therefore improving the prediction. Nevertheless, it is necessary introducing anisotropy as well as frequency dependencies in the correlation length formulation to achieve good agreements, regarding the surface pressure and far field noise spectrum, within the region of 1 kHz and higher. However, all tuning efforts seem to overpredict the far field low frequency region, mainly, due to the Von Karman spectrum used for the vertical velocity fluctuations.

Also non-symmetric airfoils have been tested, such as a NACA64418 in a combined study between the previous institutions mentioned, [42], with similar results around 1 kHz. Therefore, TNO formulation, with suitable tuning, seems to provide good estimates at high frequencies and overprediction at low frequencies, at least in a few representative airfoils used for experimental purposes or within the industry, but there is not a unique trend to predict any airfoil geometry.

3.4 Turbulent Inflow Noise

All the acoustics theory presented so far has been based on pressure fluctuations radiated as result of the scatter effect introduced by a sharp trailing edge when a turbulent flow passes nearby it. Already mentioned in the early Ffwocs analogy, in Section 3.2, at the proximities of a solid surface, turbulence radiates efficiently through an acoustic dipole instead of the expected quadrupole nature of turbulence formulated by M.J. Lighthill, [44].

As a consequence of this effect, another source of radiated noise may appear when considering a turbulent gust inflow hitting an airfoil nearby the leading edge. In this case, the interaction between the incoming inflow and the leading edge introduces a flow discontinuity which raises pressure fluctuations nearby the surface, turning into a far field radiated noise. The reader may guess that inflow turbulence noise presents the same sort of mechanism as trailing edge noise; the only difference is that turbulence is not self-generated by an airfoil boundary layer, but by incoming inflow, which is unsteady. (i.e. wake of another turbine).

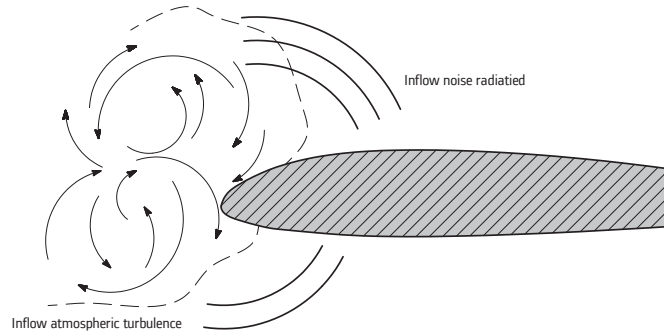


Figure 3.8: Sketch of turbulent inflow noise mechanism

Therefore, the quantification of inflow turbulence has an important effect on the radiated noise. Since turbulence possesses different length scales, it has been shown that depending on the size of turbulent eddies relative to the chord size, the inflow noise mechanism may change (i.e. $\lambda \ll c$).

When the eddy size becomes much bigger than the chord ($\lambda \gg c$), a low frequency noise is radiated scaling with the Mach number up to the 6th power. On the other hand, when the eddy size is smaller ($\lambda \ll c$) the mechanism reacts similar to an acoustic quadrupole, being less efficient than the dipole and scaling to the 5th power of the Mach number. The latter, it is the most common to be found when analysing an isolated airfoil. Being the leading edge, where this source is more noticeable as S. Oerlemans *et al.* [53] proves on isolated airfoils tested in a wind tunnel equipped with an anechoic chamber by changing drastically the turbulence intensity of incident flow.

3.4.1 Amiet's Turbulence Inflow Noise Model

Turbulence inflow main contribution was first developed by R.K. Amiet [2] based on a flat plate model. The model is formulated for a 3D plate, but it can be simplified up to a 2D case. The basic idea is that; an airfoil in a turbulent unsteady flow field experiences a fluctuating lift, as T. Theodorsen proved in his theory of unsteady aerodynamics (see the work summarised by R.L. Bisplinghoff *et al.* [13]), which according to the acoustic theories of Kirchoff and N. Curle [23] should result in a generation of sound. If the unsteady loading at each point on the airfoil is known as a function of time, then, the associated radiated sound can be calculated.

The turbulence inflow is represented by a sinusoidal 3 dimensional gust, of magnitude w_0 . Hence, the vertical component at given location of the airfoil can be written as;

$$w(x_1, x_3, t) = \int_{-\infty}^{\infty} \int_{-\infty}^{\infty} w_R(k_1, k_3) \exp(ik_1(x_1 - Ut) + k_3x_3) dk_1 dk_3 \quad (3.48)$$

where the gust has been expressed as a function of the longitudinal, k_1 , and lateral, k_3 , wavenumbers. By knowing the airfoil response to a sinusoidal gust, $g(x, k_1, k_3)$, the pressure jump at a given location of the airfoil can be computed resulting from all the wavenumbers contained within the gust;

$$\Delta P(x_1, x_3, t) = 2\pi\rho Ub \int_{-\infty}^{\infty} \int_{-\infty}^{\infty} w_R(k_1, k_3) g(x_1, k_1, k_3) \exp(ik_3x_3 - k_1Ut) dk_1 dk_3 \quad (3.49)$$

The problem is formulated for a random variable (i.e. turbulent gust), it is useful to extract the cross power density function of the pressure jump which can be developed by considering two different points on the surface;

$$S_{QQ}(x_1, y_1, \eta, \omega) = (2\pi\rho b)^2 U \int_{-\infty}^{\infty} g^*(x_1, K_1, k_3) g(y_1, K_1, k_3) \Phi_{22}(K_1, k_3) \exp(ik_2\eta) dk_3 \quad (3.50)$$

Being, $\eta = y_3 - x_3$ the distance between two points separated in the spanwise direction, $K_1 = -\omega/U$ a particular wavenumber in the chordwise direction, and Φ_{22} being the turbulence energy spectrum for the vertical velocity fluctuations. Again, under the assumption of isotropic turbulence and considering a Von Karman energy spectrum integrated along the coordinate normal to the flat plate, it yields to;

$$\Phi_{22}(k_1, k_3) = \frac{4\overline{u_2^2}}{9\pi k_e^2} \frac{(k_1/k_e)^2 + (k_3/k_e)^2}{[1 + (k_1/k_e)^2 + (k_3/k_e)^2]^{7/3}} \quad (3.51)$$

As mentioned in Section 3.3.2, k_e is the energy contained by the turbulent eddies.

The acoustic response of an unsteady loaded airfoil is determined by means of N. Curle [23] theory, distributing dipoles over the airfoil surface, with a strength equal to the force applied. The far field sound produced by a point source of strength $F(x_0, y_0, \omega) \exp(i\omega t)$ in a stream of Mach number M is defined according to R.K. Amiet [2] as;

$$P_1(x_1, x_2, x_3, \omega, x_1^*, x_3^*) = \frac{i\omega x_2 F(x_1^*, x_3^*, \omega)}{4\pi c_0 \sigma^2} \exp\left(t + \frac{M(x_1 - x_1^*) - \sigma}{c_0 \beta^2} + \frac{x_1 x_1^* + x_2 x_2^* \beta^2}{c_0 \beta^2 \sigma}\right) \quad (3.52)$$

Where $\sigma = \sqrt{x_1^2 + \beta^2(x_2^2 + x_3^2)}$ and $\beta = \sqrt{1 - M^2}$. By integrating Eq.(3.52) over the airfoil surface, and substituting it into the previous cross-PSD, Eq.(3.50), it is possible to link the far field power spectral density due to inflow turbulence pressure fluctuations with the cross-PSD of the resulting loading. Considering an infinitely large span, the following solution is obtained for a 2 dimensional flat plate;

$$\mathbf{S}_{FF}(x_1, x_2, 0, \omega) = \left(\frac{\omega x_2 \rho b}{c_0 \sigma^2}\right)^2 \pi U d |\mathfrak{L}(x_1, K_1, 0)|^2 \Phi_{22}(K_1, 0) \quad (3.53)$$

Being d the span length of the flat plate, and \mathfrak{L} representing the surface loading integral, given the response of the flat plate, g , due to an incoming harmonic gust.

$$\mathfrak{L}(x_1, K_1, k_3) = \int_{-b}^b g(x_1^*, K_1, k_3) \exp\left(-i\omega \frac{x_1^*(M - x_1/\sigma)}{c_0 \beta^2} \delta x_1^*\right) \quad (3.54)$$

R.K. Amiet [2] proves that and observer placed above a flat plate (90° with respect to the incoming flow), experiences the same acoustic radiation as if there would not be flow passing by. Basically, convective amplification is zero in such position⁶. The introduction of this assumption is essentially how the model was validated in wind tunnel testing, and

⁶The convective amplification is an additional propagation effect in aeroacoustics, based on the increase of the amplitude level due the flow convection. Usually it is quantified as a gain term of the form $1/(1 - M \cos \theta_e)^4$, being θ_e the angle in chordwise direction between source and receiver

therefore, resulting to Amiet's inflow model. Thus, by placing an observer in such a position and setting $M = 0$ to account for zero convective effects, Eq.(3.53) turns into;

$$\mathbf{S}_{FF}(0, x_2, 0, \omega) = \left(\frac{\omega \rho b}{c_0 x_2} \right)^2 \pi U d \left| \mathfrak{G} \left(\frac{\omega c}{2U} \right) \right|^2 \Phi_{22}(K_1, 0) \quad (3.55)$$

Where now, the airfoil loading is replaced by \mathfrak{G} describing the lift-response of a flat plate due to a harmonic gust as a function of a reduced frequency $\bar{\omega} = \omega c / (2U)$ and the Mach number. Although the Mach number has been set to zero in the previous step, it must be kept non-zero as it is responsible for the dipole intensity and lift response.

Airfoil's Response functions

The definition of the airfoil response functions to complete Amiet's model requires deep knowledge on unsteady aerodynamics for compressible flow. As it is not the scope of this project to focus on unsteady aerodynamics theory, only the final results presented by Amiet's are introduced and described.

Two solutions are needed, whose range of action is limited by the non-dimensional parameter $M\bar{\omega}/\beta^2$ when it is bigger or lower than $\pi/4$. The parameter can be understood as an acoustic wavelength when $M \rightarrow 0$ and $\beta \rightarrow 1$. When $M\bar{\omega}/\beta^2 < \pi/4$ a low frequency incompressible solution is used

$$\mathfrak{G}_{\text{Low}} = \left\{ \frac{1}{\beta^2} \mathfrak{S} \left(\frac{\bar{\omega}}{\beta^2} \right) \left[\mathbf{J}_0(M^2 \bar{\omega} / \beta^2) - i \mathbf{J}_1(M^2 \bar{\omega} / \beta^2) \right] \right\} \exp \left(i \frac{\bar{\omega}}{\beta^2} \mathbf{F}(M) \right) \quad (3.56)$$

Being $\mathbf{F}(M) = (1 - \beta) \log M + \beta \log(1 + \beta) - \log 2$ according to V.P. Blandeau research studies [16]. \mathfrak{S} is the well-known Sears function for a compressible flow, and J_0 and J_1 represent Bessel functions of the first kind.

On the contrary, when $M\bar{\omega}/\beta^2 > \pi/4$, a high frequency compressible solution is defined, consisting of two parts

$$\mathfrak{G}_{\text{High}} = \mathfrak{G}_1 + \mathfrak{G}_2 \quad (3.57)$$

Being the first part of the solution \mathfrak{G}_1 built from a flat plate with a semi-infinite chord and without trailing edge. While the second part, \mathfrak{G}_2 , the airfoil is modelled as a semi-infinite flat plate without leading edge. According to R.K. Amiet [2], the first terms can be modelled as follows;

$$\mathfrak{G}_1(\bar{\omega}) = \frac{1 - i}{\pi \bar{\omega} \sqrt{M}} \mathbf{E}^* \left(\sqrt{\frac{4\bar{\omega}M}{\pi(1+M)}} \right) \quad (3.58)$$

$$\begin{aligned} \mathfrak{G}_2(\bar{\omega}) = & \frac{\sqrt{1+M}}{iM(\pi\bar{\omega})^{3/2}} \left\{ \mathbf{E}^* \left(\frac{2}{\beta} \sqrt{\frac{2\bar{\omega}M}{\pi}} \right) - \right. \\ & \left. - \frac{1-i}{2} + \left[\frac{1-i}{2} - \sqrt{\frac{2}{1+M}} \mathbf{E}^* \left(\sqrt{\frac{4\bar{\omega}}{\pi(1-M)}} \right) \right] \exp^{-i2\bar{\omega}M/1-iM} \right\} \end{aligned} \quad (3.59)$$

Where \mathbf{E}^* is made of Fresnel integrals;

$$\mathbf{E}^*(x) = \int_0^x \cos\left(\frac{\pi}{2}\xi^2\right) d\xi - i \int_0^x \sin\left(\frac{\pi}{2}\xi^2\right) d\xi \quad (3.60)$$

Amiet's model is usually simplified by adopting the high frequency asymptotic behaviour of Eqs.(3.58) and (3.58), meaning that $\bar{\omega} \rightarrow \infty$. Therefore, previous expressions become;

$$\begin{aligned} \lim_{\bar{\omega} \rightarrow +\infty} \mathfrak{G}_1(\bar{\omega}) &\rightarrow \frac{-i}{\pi \bar{\omega} \sqrt{M}} \\ \lim_{\bar{\omega} \rightarrow +\infty} \mathfrak{G}_2(\bar{\omega}) &\rightarrow 0 \end{aligned}$$

By knowing the asymptotic behaviour of the airfoil response functions, it is possible to derive the far field pressure spectra expressed in one-third octave band.

Sound Pressure Level Expressions

By replacing this expression into Eq.(3.53) and assuming a Von Karman spectrum, the far field pressure fluctuations spectrum, \mathbf{G}_{FF} for the high frequency response function can be expressed in decibels as follows after some algebraic manipulations on Eq.(3.53)⁷

$$\begin{aligned} \text{SPL}_{\text{High}} [\text{dB}] &= 10 \log_{10} \left(\frac{\Lambda_2 d}{r_e^2} M^5 \frac{\bar{u}_2^2}{U^2} \frac{\widehat{K}_1^3}{(1 + \widehat{K}_1^2)^{7/3}} \right) + 10 \log_{10}(\rho^2 c_0^4) + \\ &+ 10 \log_{10} \left(2 \frac{\sqrt{\pi}}{\pi} \left(\frac{2}{3\pi} \right)^2 \frac{\Gamma(1/3)}{\Gamma(5/6)} \right) - 10 \log_{10} p_0^2 + 10 \log_{10} \left(\frac{2^k - 1}{2^{k/2}} \right) \end{aligned} \quad (3.61)$$

Being $\widehat{K}_1 = K_1/k_e$ and p_0 the standard normalisation factor for pressure levels; $p_0 = 2 \cdot 10^{-5}$ Pa. The last term from Eq.(3.61) represents the octave band factor. By forcing $k = 1/3$, Eq.(3.61) becomes the inflow turbulence sound pressure level (high frequency response) expressed in one-third octave band. Most of the previous terms from Eq.(3.61) are constant, so Eq.(3.61) is usually found in the common literature as;

$$\text{SPL}_{\text{High}} [\text{dB}] = 10 \log_{10} \left(\frac{\Lambda_2 d}{r_e^2} M^5 \frac{\bar{u}_2^2}{U^2} \frac{\widehat{K}_1^3}{(1 + \widehat{K}_1^2)^{7/3}} \right) + \underbrace{10 \log_{10}(\rho^2 c_0^4) + 78.44}_{=181.30} \quad (3.62)$$

Due to the inclusion of the Von Karman spectrum and vertical velocity fluctuations into Eq.(3.61), two new parameters have been included; the turbulence length scale, Λ_2 and the vertical velocity fluctuations, \bar{u}_2 . As there is not a unique response function covering the whole range of frequency, it is important to introduce a continuous transition between functions around $\pi/4$ must be as continuous.

Regarding the low response function defined by Eq.(3.56), M.V. Lawson [47] elaborated a formulation to include low and high frequency contributions based on R.K. Amiet's research, by including a smooth transition between both regions.

$$\text{SPL}_{\text{Total}} [\text{dB}] = \text{SPL}_{\text{High}} + 10 \log_{10} \left(\frac{\text{LFC}}{1 + \text{LFC}} \right) \quad (3.63)$$

⁷The reader must be aware of that the power spectrum density function described in Eq.(3.53) must be multiplied by two in order to account for the positive frequencies

Being LFC the low frequency response function from Eq.(3.56) approximated by the following expression;

$$\text{LFC} = 10\mathfrak{S}^2 M \frac{\bar{\omega}^2}{\beta^2} \quad (3.64)$$

The Sears function from Eq.(3.64), can be simply approximated by the following expression according to M.V. Lawson [47];

$$\mathfrak{S}^2 \left(\frac{\bar{\omega}}{\beta^2} \right) \approx \left(\frac{2\pi\bar{\omega}}{\beta^2} + \left(1 + 2.4 \frac{\bar{\omega}}{\beta^2} \right)^{-1} \right)^{-1} \quad (3.65)$$

Where $\bar{\omega}$ is the reduced frequency as mentioned before, often used when dealing with unsteady flows on airfoils.

Therefore, Amiet's model, simplified for a 2D airfoil, provides a consistent formulation for turbulent inflow noise. The main drawback of this model is the necessity of introducing the right turbulence length scale, Λ_2 , and the vertical velocity fluctuations, $\overline{u_2}$, whose modelling is still uncertain. Some authors propose the assessment of these quantities based on an airfoil basis, i.e. F. Bertagnolio [9] did it during an experimental study performed on NACA0015 wind tunnel tests. The turbulent length scale was registered for a range of wind speed from 10 to 100 m/s using difference grid layouts in the nozzle section⁸. Results show that turbulent length scale is almost constant when wind speed increases but it varies from case to case;

$$\Lambda_2 \approx 0.005 \div 0.03 \text{ m}$$

The same study was done to determine other parameters necessary for the inflow turbulence modelling, such as turbulence intensity or Kolmogorov length scale.

However, other authors assess these variables considering the overall scale of a wind turbine, being these properties equal for all the airfoils or depending on blade position. They are usually expressed as a function of surface parameters such as roughness length, z_0 . As an example, K. Boorsma *et al.* [17] proposes a model based on a ESDU standards;

$$\frac{\Lambda_2}{H} = 2 \{0.5 + 0.316(3 + \log_{10} z_0)\} \quad (3.66)$$

$$\frac{\sqrt{\overline{u_2^2}}}{U} = \frac{0.286 + 0.187 \log_{10} H - 0.081 \log_{10}^2 H}{z_0^{0.07} \log_{10} H / \log_{10} z_0} \quad (3.67)$$

W.J. Zhu *et al.* [69] also proposes a similar formulation for the turbulent scale parameter based on the roughness length, but the previous variable become a function of the height. Therefore, the position of the blade element with respect to the ground provides a different value for the turbulence intensity and length scale respectively.

The equation for the turbulence scale parameter is;

$$\Lambda_2 = 25z^{0.35} z_0^{-0.063} \quad (3.68)$$

⁸It is common to use grids in order to control the turbulence intensity of the incoming flow within the test area. Different grid layouts are used in order to generate different turbulence patterns such as high solidity, low solidity, honeycomb, etc.

Regarding the turbulence intensity, the same authors propose the following expression, again, as a function of the hub height

$$\frac{\sqrt{u_2^2}}{U} = \gamma \cdot \frac{\log(30/z_0)}{\log(z/z_0)} \quad (3.69)$$

$$\gamma = 0.24 + 0.096 \log_{10} z_0 + 0.016 \log_{10}^2 z_0$$

Using Eq.(3.68) would show that the order of magnitude of the turbulence scale parameter is now more close to atmospheric or turbine dimensions instead of local values, approximately 100-200 m depending on hub height.

Therefore, there is still a lot of discussion within the aeroacoustics community regarding which model should be used, as inflow turbulence noise is still, nowadays, a complex source mechanism to be validated in real test conditions. Mainly, it is masked by trailing edge noise, at least at low wind speeds, and secondly, it is so dependent on the atmospheric inflow conditions, which not always are measured or even known.

3.4.2 Extending Amiet Turbulence Inflow Model for Cambered Airfoils

G. Guidati *et al.* [34] developed a computational model designed for inflow turbulence noise. The model is able to predict differences in sound pressure level between different airfoil shapes, being a successful design tool for research purposes.

Although still based on simplified assumptions, the dependence between boundary layer and airfoil shape, make the method to be computational expensive, not as much as current Computational Aeroacoustics methods (CAA), but still out of scope when studying an airfoil section for different operational conditions, i.e. a wind turbine.

For that reason, P.J. Moriarty [55] in collaboration with G. Guidati designed an engineering method based on the results achieved through the computational calculations in order to introduce the differences observed in inflow turbulence noise behaviour regarding the geometry/camber of an airfoil. Correcting, in that way, the sound pressure level predicted by R.K. Amiet formulation [2], that is based purely on a flat plate model.

The idea behind this model is comparing the difference in sound pressure level between the semi-infinite flat plate and the cambered airfoil. This relation is only dependant on the Strouhal number and independent on the Mach number within the range of $\approx 0.10 \div 0.20$ according to the authors. The study also proved that the effect of camber is less important than the effect of thickness within a range of Strouhal numbers of interest, usually, lower than 100. The range that the authors consider the model to be validated is below a Strouhal number of 75. Under these conditions, the effect of camber accounts for less than 2 dB, and considering a typical operational Mach number of 0.2, the Strouhal number limits up to a frequency of 4 kHz for an airfoil chord of 0.2 m and up to 800 Hz for an airfoil chord of 1 m.

A inflow turbulence noise indicator is defined based on two thickness parameters as follows;

$$IT = t_{\text{rel},1\%} + t_{\text{rel},10\%} \quad (3.70)$$

Being $t_{\text{rel},1\%}$ the relative thickness at 1% of chord length and $t_{\text{rel},10\%}$ the relative thickness at 10% of chord length. The relation between the IT indicator and the slope of the ΔSPL

as a function of the Strouhal number seems to be quadratic for the tested airfoil used in this analysis.

The slope parameter fits best with a quadratic polynomial as a function of the inflow turbulence noise indicator, according to P.J. Moriarty *et al.* [55].

$$SL = 1.123IT + 5.317IT^2 \quad (3.71)$$

Therefore, the change in sound pressure level as a function of the Strouhal number can be modelled by means of the following equation;

$$\Delta\text{SPL}_{\text{Inflow}} [\text{dB}] = -(1.123(t_{\text{rel},1\%} + t_{\text{rel},10\%}) + 5.317(t_{\text{rel},1\%} + t_{\text{rel},10\%})^2) \left(\frac{2\pi fc}{U} + 5 \right) \quad (3.72)$$

Where the constant +5, it was added in order to achieve a better fitting amongst the results obtained from different tested airfoils, by defining a common point for all the cases. Eq.(3.72) is directly applied to the results coming from Amiet theory on a flat plate, i.e. Eq.(3.63), knowing first, the thickness features of the airfoil under analysis.

Clearly, this is an engineering model, fitted in order to reduce computational cost by using the full Guidati model. Nevertheless, the model has a limited range of validity, concerning the Mach number, what could be an inconvenience regarding current state-of-the-art turbines. Although spinning at lower rotor speed, the local Mach numbers achieved in the outer region are, nowadays, close to 0.30 as a result of the enlargement undergone by new blade designs. The usage of these model could imply operating out of the boundaries established by P.J. Moriarty *et al.* [55]. On the other hand, it can provide a quite good and quick estimation of turbulent inflow noise on wind turbine noise prediction.

Analysis of Wind Turbine Noise Measurements

This chapter is a summarised version of the original one as a result of the current Non-Disclosure Agreement established between TU Delft, DTU and Siemens Wind Power A/S.

Once the basic aeroacoustic theory applied to wind turbines has been detailed in Chapter 3, the first step in wind turbine noise modelling analysis, is focused on the information provided by experimental noise measurements recorded in real field conditions. Dedicated noise measurement data is analysed coming from different operational wind turbines, including different rotor sizes, rated power, blade technology and operational settings.

This vast range of data is used to understand how the overall sound power level of a wind turbine performs according to the operational conditions and blade features. Hence, it allows building up a simplistic physical model based on key indicators of noise radiation. Such model is going to be later compared with results achieved via more complex models already detailed in Chapter 3 in order to examine the differences observed.

Therefore, the objective of this first analysis is, basically, to have a comprehensive evaluation of wind turbine noise measurements, being nowadays, the unique way of validating aeroacoustic models when applied in a wind turbine. Moreover, measurements provide relevant information about noise within different regions of operation of a wind turbine, and so, identify the main characteristics of each regime.

4.1 Wind Turbine Steady Performance

The performance of a wind turbine can be perfectly described by its power curve as a function of the wind speed along with the control settings: rotor speed, Ω and pitch angle, θ_p . Figure 4.1a shows these three elements when calculating a standard power curve of a wind turbine.

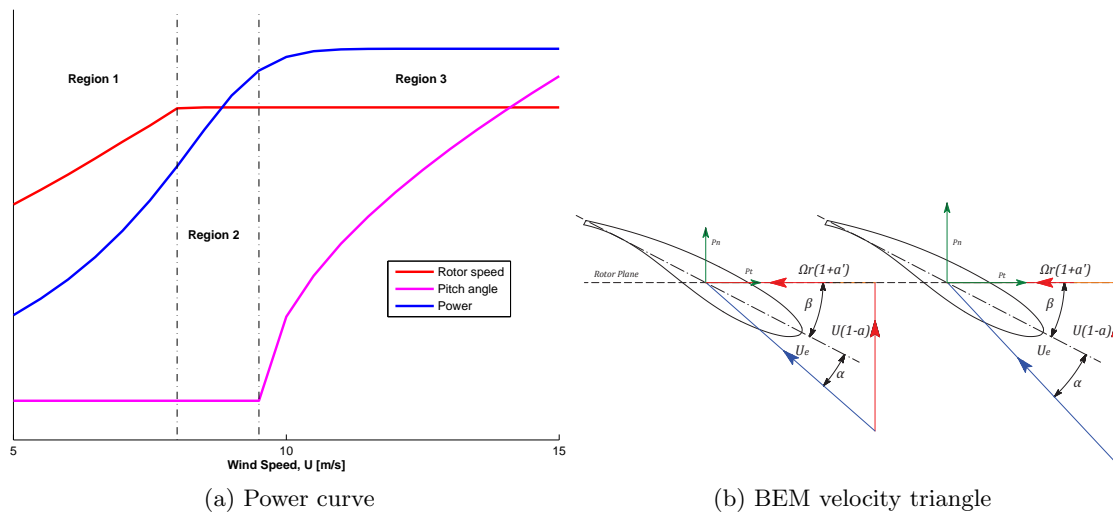


Figure 4.1: Result of a steady performance calculation. a) Power curve, b) triangle of velocities

Besides the power curve, all the information seen by each element from the blade, which can be represented by the Blade Element Momentum velocity triangle, Figure 4.1b, is also required for a local analysis. The latter is the most important for wind turbine noise assessment.

The understanding of each region from the power curve as well as the velocity triangle is crucial as it has a direct impact on how wind turbine noise behaves. Mainly, as a result of the main dependencies of the aeroacoustic models, introduced in previous Chapter 3.

4.2 Sound Power Level Experimental Measurements

Wind turbine measurements have been performed following the procedures stated in the IEC standard, IEC-61400-11 - *Wind turbines - Part 11: Acoustic noise measurement techniques* [37]. As a main outcome, wind turbine noise is measured using a microphone placed downwind the rotor aligned with the nacelle and tower baseline. Figure 4.2 clarifies the position of such microphone.

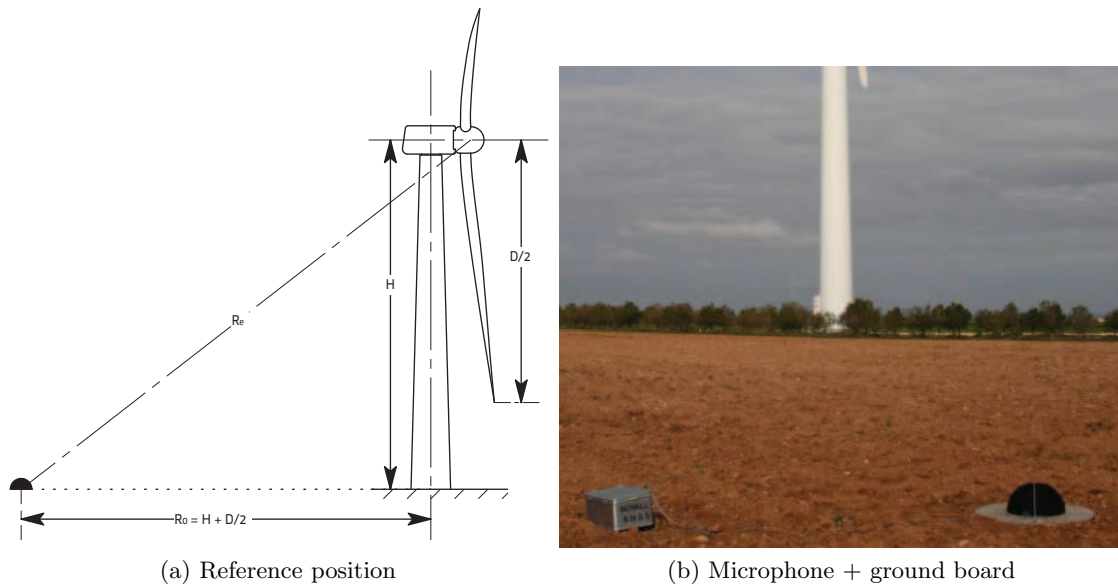


Figure 4.2: Location of the microphone that records wind turbine noise. a) Sketch extracted from IEC-61400-11, b) microphone in real field conditions

The microphone records the sound pressure level, SPL, with a threshold of $p_0 = 2 \cdot 10^{-5}$ Pa every one 1 min, according to the standard. The main drawback with this system is that, turbine noise and background are recorded when the turbine is running. Obviously, they are occurring at the same time.

Once background noise is corrected, sound pressure level is converted into sound power level at hub height by means of the following equation according to the standard, IEC-61400-11.

$$\text{SWL}_{j,\text{Turbine},A} [\text{dB}(A)] = \text{SPL}_{j,\text{Turbine},A} [\text{dB}(A)] + 10 \log_{10} \left(\frac{4\pi r_e}{S_0} \right) - 6 \quad (4.1)$$

The final spectra achieved can be seen in Figure 4.3, once corrected.

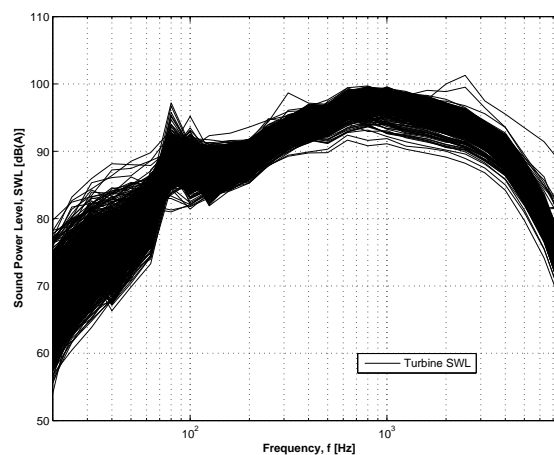


Figure 4.3: Example of a standard sound power level spectra from a wind turbine measurement

The only missing step is to filter out mechanical noise which is not of interest for this project. As a summary, mechanical noise is known by its tonal behaviour, therefore, the clear peaks detected in Figure 4.3, indicate the presence of this non-desirable source of noise, which has to be removed.

4.3 Sound Power Level Measurements Evaluation

The purpose of a deep analysis in wind turbine measurements is basically, to get a better understanding of how noise is behaving under different control operations and learn from it. It means that a model could be build from it in order to possess a method to predict wind turbine noise based purely on an empirical basis.

This analysis has been possible as a result of possessing several measurements done in different rotors. At the same time, these rotors presented different classes of blade design technology, which make it more interesting to observe differences amongst them.

After applying several statistical analysis, it has been possible to generate predictions based on the information gathered from the measurements and collapse in an empirical model, whose specific details are not shown here. This methodology is going to be validated with the other aeroacoustic models mentioned in Chapter 3 in order to understand the differences observed between measurements and theoretical predictions, as the first model resembles a closest reality regarding wind turbine noise as a whole.

Evaluation, Validation and Improvement of Aeroacoustics Models

This chapter is a summarised version of the original one as a result of the current Non-Disclosure Agreement established between TU Delft, DTU and Siemens Wind Power A/S.

Having analysed thoroughly wind turbine noise measurements from different rotors operating under different performance settings, it has provided an insight of how rotor noise (level and spectrum), behaves depending on the performance and blade design.

The physical analysis carried out in Chapter 4, shows significant differences between state-of-the-art blade designs and old designs. However, the developed empirical model cannot capture the local effects occurring as it has been based on main noise drivers defined under some assumptions to reduce modelling complexity.

Therefore, the logical step is to use the models already introduced along Chapter 3 and performing simulations using the same set of settings in order to observe current differences between models and measurements.

5.1 Introduction to Wind Turbine Prediction

The more advance aeroacoustic models introduced in Chapter 3 are based on the assessment of acoustic properties in an airfoil or local basis, summing up each of the contributions from all the elements defined by assuming that sources are non-coherent (not in phase). For that reason it is important to possess reliable information of the flow properties on an airfoil basis.

Figure 5.1 shows a sketch of how a typical distribution of sources would be located on a single blade element.

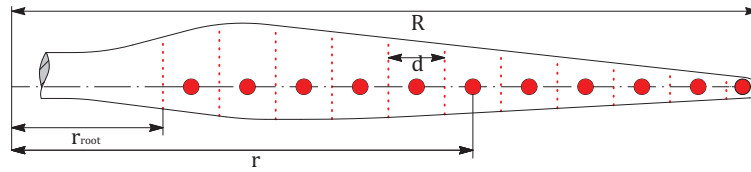


Figure 5.1: Sketch of a blade with their corresponding noise sources distributed along the spanwise direction for a defined number of sections

There is not existing model that allows a full 3D calculation of noise radiation. For that, it would be necessary a full CAA calculation, whose state-of-art-performance is still on airfoil basis as well.

There are two different ways to evaluate sound power level. Either calculate it straight forward on the blade, by assuming that all blades behave equally¹, and sum all the source at a hub height as sound power level. Or, propagate noise for each source up to a receiver point, considering all the effects involved on that, and sum all contributions as sound pressure level. Later on, it is converted back to sound power level on a representative point of the turbine (i.e. hub height). Figure 5.2 shows a representation of both methods.

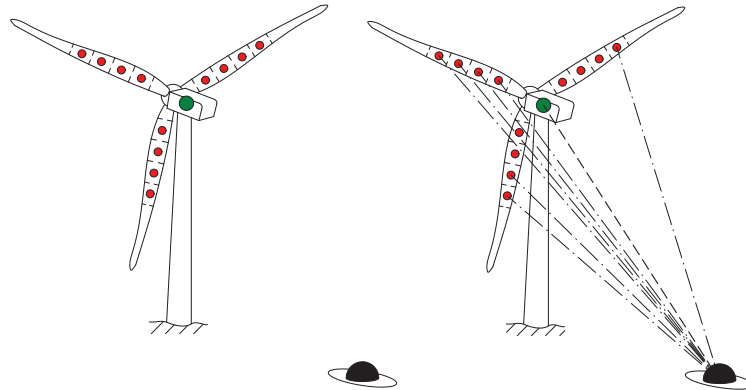


Figure 5.2: Representation of noise sound power level modes. a) Sound power level is assessed directly on the blades (red spots) and considered equal for each blade. b) Sound pressure level is assessed at a receiver position, adding the contribution of each blade and propagating it back (dash bold line) to hub height (green spot)

At the end, to perform an evaluation and improvement study in this section, the first scenario has been chosen. Although not modelling a full reality, the elements involved are better controlled than just introducing more complexity, which makes difficult to trace the source of uncertainties and problems.

¹Notice that wind shear assumption is not considered.

5.2 Evaluation and Improvement of Aeroacoustics Models Against Measurements

A consistent analysis has been performed by checking first the assumptions done when creating the empirical model used in Chapter 4. This time, the check has been done using aeroacoustic models. By doing such a simple check, it could be possible to observe and understand clearly the difference between real measurements and theoretical predictions.

That has been the first step to question why there have been such differences, or from where could they come. Actually, a crucial milestone in this project as a result of the start-up perspective: the analysis of wind turbine noise measurements.

Further steps have been based on digging on the models and identify the reasons of such differences, followed by mathematical corrections that mainly have reduced the uncertainties associated to them when compared to the measurements. Such corrections are not stated here, but the final output of the predictions, both, in spectra and overall level reduces the uncertainty with respect to their corresponding measurements. Obviously, differences are still present, especially, as a result of the difficulties to model the physics behind wind turbine noise spectrum.

Nevertheless, it is important to outline the results achieved that improve significantly the predictions done in different turbines. Having a reliable model that predicts better the reality, or at least, it gets closest, it is a clear advantage as it can be used for further steps during the design of a new wind turbine prototypes. This aspect is going to be tested in the following chapter.

Design of Low-Noise Optimised Control Settings

This chapter is a summarised version of the original one as a result of the current Non-Disclosure Agreement established between TU Delft, DTU and Siemens Wind Power A/S.

After having improved the acoustic or semi-empirical models for wind turbine noise and having achieved good agreements in the overall levels and spectra, it is time to study, in depth, the performance of a wind turbine "noise-wise".

Not only the scope of this chapter is going to show what is the noise response as a result of a specific performance, but also how the existent performance of a wind turbine can be optimised, energy-wise, given a certain noise constraint.

At this point of the project, the reader must be familiar that without the use extra add-ons on the blades, the reduction of noise is achieved, mostly, by a loss in power production, mainly, as a result of the direct relation between rotor speed and noise, but also due to performance constraints. A simple rule of a thumb for a given rotor configuration could be: the greater the power achieved, the greater noise. However, not always it should be like this.

So the question here to be discussed is whether it is possible to find an optimal performance, in terms of power generation, given a certain constrained noise level. For example, "Is it possible to extract more power under a noise constraint of -3dB with respect to the standard operation?"

6.1 Noise and Power Performance Spaces

The main objective here is to optimise the performance of a wind turbine when fixing a given noise level. So the intention of this methodology is, basically, to plan wisely new strategies while achieving the maximum performance for the wind turbine.

The indicator to maximise is the Annual Energy Production, AEP, that comes from combining the power curve of a turbine and the probability distribution of wind speed for

a given site, usually represented by a Rayleigh (1-DOF) or Weibull (2-DOF) pdf. Figure 6.1 provides a first idea of how AEP is assessed.

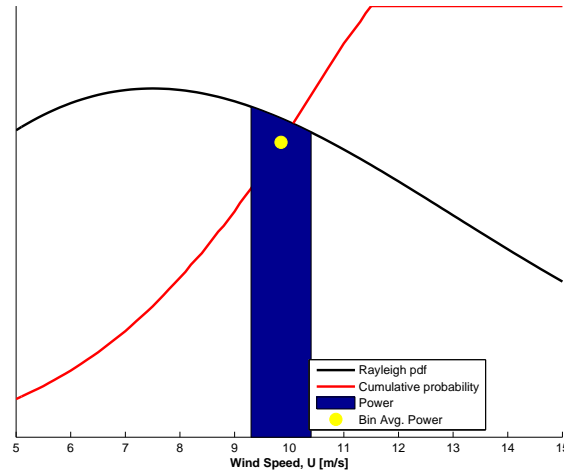


Figure 6.1: Annual energy production calculation

Figure 6.1 can be also summarised by the following equation.

$$\text{AEP [MWh]} = 8760 \sum_{i=1}^N \bar{P}_i(U_i) \cdot F_{U,\text{Rayleigh}}(U_i, U_{\text{avg}}) \quad (6.1)$$

Being $F_{U,\text{Rayleigh}}(U_i, U_{\text{avg}})$, the cumulative Rayleigh distribution, and U_{avg} the averaged wind speed at a site, required parameter for using a Rayleigh distribution.

Besides, the constraint functions are also needed in order to solve the problem. The first and most important, it is prescribing the noise level as a function of the wind speed. The other constraint refers to the maximum allowable power/torque. If a reduction of rpm is applied, it might not be possible to keep the same power, as the generator has its own limitations.

The result of the optimisation must be a pair of settings (rotor speed and pitch angle) for each wind speed considered in the analysis up to covering the standard range for a noise curve.

At the end of this analysis, repeated for each wind speed, it is possible to obtain a power curve based on the control settings (rotor speed and pitch angle) extracted from the optimisation. From that point, the calculation of the AEP is straight forward, as described by Eq.(6.1).

The remaining question is whether a turbine running with such settings behaves as predicted by the noise models.

6.2 Validating Low-Noise Settings with Field Measurements

Unfortunately, the noise validation with the new optimised settings, could not be accomplished in the frame of this project as a result of multiple drawbacks that occurred when

performing the tests. Noise tests are usually performed in uncontrolled environment and a lot of effects can alter the final output. In this case, signal-to-noise ratio were not high enough to have a good validation.

Research Conclusions

This chapter is a summarised version of the original one as a result of the current Non-Disclosure Agreement established between TU Delft, DTU and Siemens Wind Power A/S.

The end of this project has been reached by covering all the aspects initially scoped in Chapter 1. Obviously, the topics analysed along this document have been more or less successful, according to the results achieved, given the amount of time and resources initially considered to carry out the mentioned tasks.

Here, the main conclusions of this project are exposed. However, it is also a space for critics, specially, to outline the unsolved questions that, unfortunately, remain to be answered due to the lack of data. Moreover, recommendations for further research are going to be drawn as it is expected that this project may contribute actively within wind turbine noise research and aeroacoustics community.

7.1 Main Contributions of this Thesis

The main objective of this thesis research has been to investigate and understand wind turbine noise, and being able to introduce modifications in existing models based on an intensive analysis in experimental measurement, and therefore reduce uncertainties typically found on them. That is the main picture that has tried to deal with along this thesis. The main results, achieved along these chapters, are going to be summarised below these lines.

Starting from the analysis of current state-of-the-art in wind turbine noise, several efforts during last decades have been done to understand and model wind turbine noise from a physical point of view. Research proved that there are still too many unknowns and uncertainties associated to wind turbine noise, specially, as a result of the uncontrollable conditions usually found in field conditions, an aspect that has been possible to visualise in this document, i.e. Chapter 4. State-of-the-art clearly shows how the scientific community is still struggling against understanding aerodynamic noise brought to complex systems

such as wind turbine rather than on an airfoil basis. Therefore, this situation has given space to bring new ideas or challenge the models.

The first contribution of this thesis has been the analysis of wind turbine noise measurements, Chapter 4, coming from different rotors of Siemens Wind Power with different state-of-art blade technology. Data has been analysed in order to find trends based on main noise drivers. The trends found, in overall level only, allow predicting wind turbine noise for different rotor features identified in Siemens Wind Power rotors. Besides the particular features identified in Siemens Wind Power blades, the usage of a pure empirical model to predict wind turbine noise has provided significant and important results, showing a closer reality than most of the measurements included.

This experimental approach has provided more than a simple way to understand wind turbine noise, in terms of overall level, and even predict it. Basically, it has led to the second main contribution of this project, by establishing the basis to identify the weaknesses of more advanced and complicated models, outlined already in Chapter 3, and later applied in Chapter 5. All what has been learnt from the experimental results, it has been translated into more advance aeroacoustic models.

Mathematical modelling has been applied in the definition of the aeroacoustic models by giving them a more physical relevance to those effects that radiate noise (i.e. boundary layer displacement thickness on the suction side), and at the same time, be able to perform predictions in spectrum and overall level under any operation, even stall. Improvements have provided outstanding results as shown in Chapter 5, although further work is still required.

Finally, once the acoustic models have been improved, the project has focused on a more operational perspective covering the third and last contribution of this thesis. Chapter 6 has proposed a way to combine an acoustic model with a power performance model in the quest for extracting maximum energy (AEP), once a noise constraint has given. In other words, determine the way that a turbine can operate best once noise is fixed.

A case study has been chosen whose objective has been to determine a new -3dB strategy. Several solutions have been found, according to different operational constraints that provide more AEP than the existing one. A noise campaign has been performed in order to test whether models are aligned with reality or not. Unfortunately, as seen in Section 6.2, a full validation could not be achieved as a result of the unpredictable difficulties experienced during the field measurements; wrong performance, measurements affected by birds, roads, etc. Therefore, further tests are going to be performed, now, out of this project frame so as to validate whether the assumptions considered during the optimisation are valid.

As it can be seen, this project has fulfilled most of the scope initially set up, achieving relevant results along the course which have had an important impact for the development of it. This project concludes with the satisfaction that the know-how in wind turbine noise has been substantially increased, and it is expected or desired that the topics here outlined may open new lines in the aeroacoustics research field.

7.2 Suggestions for Further Research

Unfortunately, not everything has been able to solve. Given the time constraints, and most important, the available data, some aspects could not be answered as expected. This section tries to summarise them by doing some criticism and, indeed, provide some recommendations for further research.

One of the hot topics discussed along this report has been inflow turbulence noise. Postulated as an important source of noise in the literature, it is and has been seldom to find evidence in the considered measurements, as there has been a high agreement between them and when using acoustic models without it.

It is true, though, that the information required to model inflow noise, has not been available, and missing in every single measurement here considered. Certainly, it is referred to vertical velocity fluctuations, $\overline{u_2^2}$, and the turbulence length scale, Λ_2 . These two variables define the classical inflow turbulent noise problem postulated by R.K. Amiet [2] along with other parameters. Measurements carried out could not acquire these two variables that, at least, could provide a better estimate that just using a random value.

The other difficulty is that inflow turbulence noise may occur at low frequencies, typically where background noise usually overlaps turbine noise. Besides, A-Weighted penalises the behaviour at the low frequency region. For that reason, it has been also hard to model properly this part of the spectrum. Measurements, as shown in Chapter 5, seem to indicate, even with A-Weighting, that extra noise is generated at lower frequencies. Nevertheless, without proper evidence, it cannot be justified.

Similar studies such as the one carried out by H.Aa. Madsen *et al.* [49] could be the key to study and characterize inflow turbine noise, by using surface pressure microphones coupled, probably, with standard standalone downwind microphone. Besides, having a met. mast of a considerable height, $70 \div 100$ m, would also reduce the uncertainty of incoming wind speed, instead of using, typically, the 10m met. mast or nacelle anemometer. Wind shear profile could be also included, as a uniform wind profile has been assumed in the whole report. The proper characterization of the wind shear could explain better the trends and scatter observed in Chapter 4.

Indeed, some of the ideas introduced along this thesis have been based on specific measurements coming from Siemens Wind Power designs. Obviously, there are not claimed to be a unique solution, as some of the modifications try to reproduce trends extracted from observations, but to recreate a reality. However, all the changes introduced must be seen as a way to challenge the models, when brought to wind turbine scales. Therefore, these results should be taken in consideration in the quest for improving wind turbine noise modelling.

Nevertheless, more effort has to be invested in spectra modelling in order to achieve better predictions, turbine wise. Measurement analysis was focussed only in the overall level, but not in the spectra. It could be interesting to investigate normalised spectral shapes using the same noise drivers from Chapter 4.2. As a future request, keep introducing changes in the models and include inflow noise if evidence is found.

References

- [1] *NordTest Method NT Acou 107 Approved 2001-05. Acoustics: A Framework for the Verification of Environmental Noise Calculation Software*, 2002.
- [2] R.K. Amiet. Acoustic radiation from an airfoil in a turbulent stream. *Journal of Sound and Vibration*, 41(4):407–420, 1975.
- [3] R.K. Amiet. Noise due to turbulent flow past a trailing edge. *Journal of Sound and Vibration*, 47(3):387–393, 1976.
- [4] J.D. Anderson Jr. *Fundamentals of Aerodynamics*. McGraw-Hill Companies, Inc., 2011. ISBN 978-007-128908-5.
- [5] J. Ask and L. Davidson. Flow and dipole source evaluation of a generic sub. *Journal of Fluids Engineering*, 132(5), 2010.
- [6] R. Bareiß, G. Guidati, and S. Wagner. Codes as a basis for aerodynamic noise prediction of horizontal axis wind turbines. In *Proceedings of European Wind Energy Conference*, 1993.
- [7] H.E. Bass, L.C. Sutherland, and A.J. Zuckerwar. Atmospheric absorption of sound: Update. *Journal of Acoustical Society of America*, 88(2019), 1990.
- [8] H.E. Bass, L.C. Sutherland, A.J. Zuckerwar, D.T. Blackstock, and D.M. Hester. Atmospheric absorption of sound: Further developments. *Journal of Acoustical Society of America*, 97(680), 1995.
- [9] F. Bertagnolio. Naca0015 measurements in 1m wind tunnel and turbulence generated noise. Technical Report Risø-R-1657(EN), DTU-Risø National Laboratory, 2008.
- [10] F. Bertagnolio. Trailing edge noise model applied to wind turbine airfoils. Technical report, DTU-Risø National Laboratory, 2008.
- [11] F. Bertagnolio, H.Aa. Madsen, and C. Bak. Experimental validation of the trailing edge noise model and application to airfoil optimization. In *Conference Proceedings EWECE*, 2009.

- [12] F. Bertagnolio, A. Fischer, and W.J. Zhu. Tuning of turbulent boundary layer anisotropy for improved surface pressure and trailing-edge noise modeling. *Journal of Sound and Vibration*, 333(1):991–1010, 2014.
- [13] R.L. Bisplinghoff and H. Ashley. *Principles of Aeroelasticity*. Dover-Phoneix Editions, 1962. ISBN 0-486-49500-0.
- [14] W.K. Blake. *Mechanics of flow-induced sound and vibration*. Frenkiel, F.N. and Temple, G., 1986.
- [15] V.P. Blandeau and P.F. Joseph. Validity of amiet’s model for propeller trailing-edge noise. *AIAA Journal*, 2011.
- [16] V.P. Blandeau, P.F. Joseph, and G. Gabard. Sound power radiation due to an isolated airfoil in a turbulent stream. In *20th International Congress on Acoustics*, 2010.
- [17] K. Boorsma and J.G. Schepers. Enhanced wind turbine noise prediction tool silant. Technical Report ECN-M-12-004, Energy Research Centre of the Netherlands, ECN, 2011.
- [18] J. Bosschers, B. Montgomerie, A.J. Brand, and R.P.J.O.M van Rooy. Influence of blade rotation on the sectional aerodynamics of rotational blades. Technical report, NLR, 1996.
- [19] D. Bowdler and G. Leventhall, editors. *Wind Turbine Noise*. Multi-Science Publishing Co. Ltd, 2011. ISBN 978-1-907132-30-9.
- [20] K.S. Brentner and F. Farassat. An analytical comparison of the acoustic analogy and kirchhoff formulation for moving surfaces. *AIAA Journal*, 1998.
- [21] T.F. Brooks and T.H. Hodgson. Trailing edge noise prediction from measured surface pressures. *Journal of Sound and Vibration*, 78(1):69–117, 1981.
- [22] T.F. Brooks, D. Stuart Pope, and M.A. Marcolini. Airfoil self-noise and prediction. Technical Report NASA reference publication 1218, Langley Research Center, 1989.
- [23] N. Curle. The influence of solid boundaries upon aerodynamic sound. *Proceedings of the Royal Society of London*, 231:505–514, 1955.
- [24] W.B. De Wolf. Een predictiemethode voor het aerodynamische geluid van windturibnes met horizontale. Technical report, National Aerospace Laboratory of the Netherlands, 1986.
- [25] M. Drela. Xfoil: An analysis and design system for low reynolds number airfoils. In *Conference on low reynolds number aerodynamics*, 1989.
- [26] J.E. Ffowcs-Williams and L.H. Hall. Aerodynamic sound generation by turbulent flow in the vicinity of a scattering half plane. *Journal of Fluid Mechanics*, 40(4): 657–670, 1970.

- [27] J.E. Ffowcs-Williams and D.L. Hawkings. Sound generation by turbulence and surfaces in arbitrary motion. *Proceedings of the Royal Society of London*, 264:321–342, 1969.
- [28] K. Fowler, E. Koppen, and K. Matthis. International legislation and regulations for wind turbine noise. In *5th International Conference on Wind Turbine Noise*, 2013.
- [29] P. Fuglsang and H.Aa. Madsen. Implementation and verification of an aeroacoustic noise prediction model for wind turbines. Technical Report Risø-R-867, Risø National Laboratory for Sustainable Energy, 1996.
- [30] J. Gill, X. Zhang, P.F. Joseph, and T. Node-Langlois. Effects of real airfoil geometry on leading edge gust interaction noise. In *19th AIAA/CEAS Aeroacoustics Conference Proceedings*, 2013.
- [31] S.A.L. Glegg, S.M. Baxter, and A.G. Glendinning. The prediction of broadband noise from wind turbines. *Journal of Sound and Vibration*, 118(2):217–239, 1987.
- [32] M.E. Goldstein. The evolution of tollmien-schlichting waves near the leading edge. Technical report, Lewis Research Center, NASA, 2006.
- [33] F.W. Grosveld. Prediction of broadband noise from horizontal axis wind turbines. *Journal of Propulsion and Power*, 1(4):292–299, 1985.
- [34] G. Guidati. *Berechnung und Verminderung von Strömungsgeräuschen an Profilen*. PhD thesis, Institute of Aerodynamics and Gasdynamics, University of Stuttgart, 2003.
- [35] M. Howe. A review of the theory of trailing edge noise. *Journal of sound and vibration*, 61(3):437–465, 1978.
- [36] M. Howe. Aerodynamic noise of a serrated trailing edge. *Journal of Fluids and Structures*, 1990.
- [37] *IEC-61400-11. Wind turbines - Part 11: Acoustic noise measurement techniques*. International Electrotechnical Commission, IEC, 3rd edition, 2012.
- [38] *ISO 9613-2. Acoustics of sound during propagation outdoors - Part 2: General Method of Calculation*. ISO, 1996.
- [39] M. Kamruzzaman. *Study of turbulence anisotropy and its impact on flow induced noise emission*. PhD thesis, Institute of Aerodynamics and Gas Dynamics, University of Stuttgart, 2011.
- [40] M. Kamruzzaman, A. Herrig, W. Lutz, Th. Würz, E. Kämer, and S. Wagner. Comprehensive evaluation and assessment of trailing edge noise prediction based on dedicated measurements. *Noise Control Engineering Journal*, 59(1):54–67, 2011.
- [41] M. Kamruzzaman, Th. Lutz, K. Nübblers, and E. Krämer. Implementation and verification of an aeroacoustic wind turbine blade analysis tool. Forth International Meeting on Wind Turbine Noise, Rome, 2011.

- [42] M. Kamruzzaman, Th. Lutz, W. Würz, W.Z. Shen, W.J. Zhu, M.O. Hansen, F. Bertagnolio, and H.Aa. Madsen. *Validations and improvements of aeroacoustic models using detailed experimental data*. *Wind Energy*, 15(1):45–61, 2012.
- [43] J. Larsson, L. Davidson, L. Eriksson, and M. Olsson. Aeroacoustic investigation of an open cavity at low mach number. *AIAA Journal*, 42:2462–2473, 2004.
- [44] M.J. Lighthill. On sound generated aerodynamically i. general theory. *Proceedings of the Royal Society London*, 211(1107):564587, 1952.
- [45] M.J. Lighthill. On sound generated aerodynamically ii. turbulence as a source of sound. *Proceedings of the Royal Society London*, 222(1148):1–32, 1954.
- [46] V. Lorenzoni, M. Tuinstra, and F. Scarano. On the use of time-resolved particle image velocimetry for the investigation of rod-airfoil aeroacoustics. *Journal of Sound and Vibration*, 331(23):5012–5027, 2012.
- [47] M.V. Lowson. New prediction model for wind turbine noise. In *Proceedings of the Conference on Renewable Energy - Clean Power 2001*, volume 2, pages 177–182, 1993.
- [48] Th. Lutz, A. Herrig, W. Würz, M. Kamruzzaman, and E. Krämer. Design and wind-tunnel verification of low-noise airfoils for wind turbines. *AIAA Journal*, 45(4): 779–785, 2007.
- [49] H. Aa. Madsen, F. Bertagnolio, and A. Fischer. Measurement of high frequency surface pressure fluctuations for blade noise characterization. In *Conference on Wind Turbine and Vibration Control*, 2012.
- [50] P. Malam, K. Suluksna, and E. Justasaro. Calibrating the $\gamma - re_{\theta}$ transition model for commercial cfd. In *47th AIAA Aerospace Science Meeting*.
- [51] J.F. Manwell, J.G. McGowan, and A.L. Rogers. *Wind Energy Explained. Theory, Design and Application*. John Wiley and Sons, 2nd edition, 2009. ISBN 978-0-470-69975-1.
- [52] P.J. Moriarty. A program for calculating 2d airfoil noise. design code. Technical report, National Wind Technology Center, NREL, 2013.
- [53] P.J. Moriarty and S. Oerlemans. Wind tunnel aeroacoustic tests of six airfoils for use on small wind turbines. In *42nd AIAA Aerospace Science Meeting and Exhibit*, 2004.
- [54] P.J. Moriarty, G. Guidati, and P.G. Migliore. Recent improvement of a semi-empirical aeroacoustic prediction code for wind turbines. In *Collection of Technical Papers - 10th AIAA/CEAS Aeroacoustics Conference*, volume 3, pages 2742–2757, 2004.
- [55] P.J. Moriarty, G. Guidati, and P.G. Migliore. Prediction of turbulent inflow and trailing-edge noise for wind turbines. In *26th AIAA Aeroacoustics Conference Proceedings*, 2005.

- [56] P.J. Moriarty, G. Guidati, and P.G. Migliore. Prediction of turbulent inflow and trailing-edge noise for wind turbines. In *Collection of Technical Papers - 11th AIAA/CEAS Aeroacoustics Conference*, volume 2, pages 2742–2757, 2005.
- [57] S. Oerlemans, P. Sijtsma, and B. Méndez López. Localisation and quantification of noise sources on a wind turbine. *Journal of Sound and Vibration*, 299(4-5):869–883, 2007.
- [58] S. Oerlemans, M. Fisher, T. Maeder, and K. Kögler. Reduction of wind turbine noise using optimized airfoils and trailing-edge serrations. *AIAA Journal*, 47(6):1470–1481, 2009.
- [59] R. Parchen. Progress report draw, a prediction scheme for trailing-edge noise based on detailed boundary-layer characteristics. Technical report, TNO Institute of Applied Physics, 1998.
- [60] S. Pröbsting, F. Scarano, M. Bernardini, and S. Pirozzoli. A comparative study of turbulent boundary layer wall pressure fluctuations obtained from high-speed tomographic piv and dns. In *Proceedings of the 16th international conference on application of laser techniques to fluid mechanics*, pages 1–13, 2012.
- [61] D. Ragni, B.W. van Oudheusden, and F. Scarano. 3d pressure imaging of an aircraft propeller blade-tip flow by phase-locked stereoscopic piv. *Experimental in Fluids*, 52(2):463–477, 2012.
- [62] A.L. Rogers, J.F. Manwell, and S. Wright. Wind turbine acoustic noise. Technical report, Renewable Energy Research Laboratory, University of Massachusetts, 2002.
- [63] J.G. Schepers, A. Curves, S. Oerlemans, K. Braun, T. Lutz, A. Herrig, W. Würz, M. Mantesanz, L. Garcillán, M. Fischer, K. Kögler, and T. Maeder. Sirocco: Silent rotors by acoustic optimization. Technical Report ECN-M-07-064, Energy Research Centre of the Netherlands, ECN, 2007.
- [64] B.M. Sumer and J. Fredsøe. *Hydrodynamics around Cylindrical Structures*. Technical University of Denmark, 1997.
- [65] C. Tam. Computational aeroacoustics: An overview of computational challenges and applications. *International Journal of Computational Fluid Dynamics*, 18(6):547–567, 2004.
- [66] I. Troen and E.L. Petersen. *European Wind Atlas*. Risø National Laboratory, Roskilde, 1998.
- [67] C. Tsai, L. Fu, C. Tai, Y. Huang, and J. Leong. Computational aero-acoustic analysis of a passenger car with a rear spoiler. *Applied Mathematical Modelling*, 33(9):3661–3673, 2009.
- [68] S. Wagner, R. Bareiß, and G. Guidati. *Wind Turbine Noise*. Springer-Verlag Berlin Heidelberg, 1996. ISBN 978-3-642-88710-9.
- [69] W.J. Zhu, N. Heilskov, W.Z. Shen, and J.N. Sørensen. Modelling of aerodynamically generated noise from wind turbines. *Journal of Solar Energy Engineering*, 127(4):517–528, 2005.

Appendix A

Octave Bands

The range of frequencies of interest is the audible range which goes from 20 Hz to 20 kHz. Although it is possible to carry out an analysis of a source on a frequency basis, in most cases, it is impractical and time-consuming. Instead of it, a scale of octave bands and one-third of octave bands are widely used amongst the acoustics community.

A.1 Definition

Each band covers a specific range of frequencies and excludes the rest of them. If f_n represents the lower cut off frequency for a specific band and f_{n+1} the upper cut off frequency, the ratio of band limits is given by;

$$f_{n+1} = 2^k f_n \quad (\text{A.1})$$

Where, $k = 1$ for full octave bands and $k = 1/3$ for one-third octave bands. The central frequency of a specific band is $2^{k/2}$ times the lower cut off frequency;

$$f_0 = 2^{k/2} f_n \quad (\text{A.2})$$

And the band width is defined as;

$$\text{BW} = f_{n+1} - f_n \quad (\text{A.3})$$

Combining Eqs.(A.1) and (A.2) into Eq.(A.3), the bandwidth can be expressed as a function of the central frequency, f_0 , as follows;

$$\text{BW} = \frac{2^k - 1}{2^{k/2}} f_0 \quad (\text{A.4})$$

Table A.1 shows the whole range of frequencies inside the audible range expressed in one-third octave band and one octave band. The lower and upper frequencies that define the central frequency of the band are also displayed.

Table A.1: Left) Audible range expressed in one-third octave band. Right) Audible range expressed in one-octave band

One-Third Octave Band			One Octave Band		
Lower cut off frequency [Hz]	Central frequency [Hz]	Upper cut off frequency [Hz]	Lower cut off frequency [Hz]	Central frequency [Hz]	Upper cut off frequency [Hz]
14.25	16	17.96	11.00	16	22.00
17.96	20	22.63	-	-	-
22.63	25	28.51	-	-	-
28.51	32	35.92	22.00	31.5	44.00
35.92	40	45.25	-	-	-
45.25	50	57.02	-	-	-
57.02	63	71.84	44.00	63	88.00
71.84	80	90.51	-	-	-
90.51	100	114.04	-	-	-
114.04	125	143.68	88.00	125	176.00
143.68	160	181.02	-	-	-
181.02	200	228.07	-	-	-
228.07	250	287.35	176.00	250	352.00
287.35	315	362.04	-	-	-
362.04	400	456.14	-	-	-
456.14	500	574.70	352.00	500	704.00
574.70	630	724.08	-	-	-
724.08	800	912.28	-	-	-
912.28	1000	1149.40	704.00	1000	1408.00
1149.40	1250	1448.15	-	-	-
1448.15	1600	1824.56	-	-	-
1824.56	2000	2298.80	1408.00	2000	2816.00
2298.80	2500	2896.31	-	-	-
2896.31	3150	3649.12	-	-	-
3649.12	4000	4597.60	2816.00	4000	5632.00
4597.60	5000	5792.62	-	-	-
5792.62	6300	7298.24	-	-	-
7298.24	8000	9195.21	5632.00	8000	11264.00
9195.21	10000	11585.24	-	-	-
11585.24	12500	14596.48	-	-	-
14596.48	16000	18390.42	11264.00	16000	22528.00
18390.42	20000	23170.48	-	-	-

A.2 Octave Band Conversion

It is usually interesting converting amplitudes that are registered on one-third octave bands into one octave bands, the conversion can be done by means of applying the loga-

rithmic addition rule whose formula is described as follows;

$$L_{1-\text{Oct}} [\text{dB}]_i = 10 \log_{10} \left(10^{L_{1/3-\text{Oct}} [\text{dB}]_{i-1}/10} + 10^{L_{1/3-\text{Oct}} [\text{dB}]_i/10} + 10^{L_{1/3-\text{Oct}} [\text{dB}]_{i+1}/10} \right) \quad (\text{A.5})$$

Being $L_{1-\text{Oct}}$ the amplitude expressed in one octave band. In Table A.2, there is an example of how the conversion is done for a given frequency in the one octave band spectrum.

Table A.2: Conversion from one-third octave band levels to one octave band levels.

One-Third Octave Band		One Octave Band	
Frequency [Hz]	SPL [dB]	Frequency [Hz]	SPL [dB]
50	67.811	-	-
63	72.234	63	77.690
80	75.561	-	-

Where;

$$\text{SPL}_{f=63 [\text{Hz}]} [\text{dB}] = 10 \log_{10} \left(10^{67.811/10} + 10^{72.234/10} + 10^{75.561/10} \right) = 77.690 [\text{dB}]$$

The Brooks, Pope and Marcolini model. Detailed Formulation

B.1 Turbulent Boundary Layer Trailing Edge Noise, TBL-TE

In the turbulent boundary layer trailing edge noise case, the scaling law expressed in sound pressure level must be modelled for each contribution. In particular, for low angles of attack, three sources contribute. Those are the pressure side contribution, the suction side and the separated flow or AoA term. According to T.F. Brooks *et al.* [22];

- Pressure side term;

$$\text{SPL}_p[\text{dB}] = 10 \log_{10} \left(\frac{\delta_p^* M^5 d \bar{D}_H}{r_e^2} \right) + \mathbf{A} \left(\frac{\text{St}_p}{\text{St}_1} \right) + (K_1 - 3) + \Delta K_1 \quad (\text{B.1})$$

- Suction side term;

$$\text{SPL}_s[\text{dB}] = 10 \log_{10} \left(\frac{\delta_s^* M^5 d \bar{D}_H}{r_e^2} \right) + \mathbf{A} \left(\frac{\text{St}_s}{\text{St}_1} \right) + (K_1 - 3) \quad (\text{B.2})$$

- Separation or AoA term;

$$\text{SPL}_\alpha[\text{dB}] = 10 \log_{10} \left(\frac{\delta_s^* M^5 d \bar{D}_H}{r_e^2} \right) + \mathbf{B} \left(\frac{\text{St}_s}{\text{St}_2} \right) + K_2 \quad (\text{B.3})$$

The total contribution is obtained by applying the logarithmic addition rule as follows;

$$\text{SPL}_{\text{TBL-TE}}[\text{dB}] = 10 \log_{10} \left(10^{\text{SPL}_p/10} + 10^{\text{SPL}_s/10} + 10^{\text{SPL}_\alpha/10} \right) \text{ if } \alpha < 12.5^\circ \quad (\text{B.4})$$

The Strouhal numbers that appear on Eqs.(B.1), (B.2) and (B.3) must be referred at the characteristic length scale for each case, in fact, boundary layer displacement thickness seems to give a better approach than simply using boundary layer thickness.

$$St_p = \frac{f\delta_p^*}{U_e} \quad (B.5)$$

$$St_s = \frac{f\delta_s^*}{U_e} \quad (B.6)$$

The rest of Strouhal numbers are based on Mach number dependence as well as angle of attack as Eqs.(B.7) and (B.8) show;

$$St_1 = 0.02M^{-0.6} \quad (B.7)$$

$$St_2 = St_1 \cdot \begin{cases} 1 & \text{for } \alpha < 1.33^\circ \\ 10^{0.0054(\alpha-1.33)^2} & \text{for } 1.33^\circ \leq \alpha < 12.5^\circ \\ 4.72 & \text{for } \alpha \geq 12.5^\circ \end{cases} \quad (B.8)$$

St_2 has been tested to applied better to the separation flow contribution rather than St_1 . However, it is sometimes convenient replace St_1 for \overline{St}_1 at the suction side contribution. Where;

$$\overline{St}_1 = \frac{1}{2} (St_1 + St_2) \quad (B.9)$$

With respect to the spectral functions A and B, tests carried out on NACA 0012, brought several expressions as a function of the ratio Strouhal number to its peak value which can be, depending on the case of analysis, St_1 , St_2 or \overline{St}_1

Defining the a parameter as $a = |\log_{10} (St/St_{\text{peak}})|$, where; $St = [St_p, St_s]$ and $St_{\text{peak}} = [St_1, St_2, \overline{St}_1]$. Tests provided the maximum and minimum value of A, any other value must be interpolated by applying the subsequent equations.

$$A_{\min}(a) = \begin{cases} \sqrt{67.55 - 886.79a^2} - 8.22 & \text{for } a < 0.204 \\ -32.67a + 3.98 & \text{for } 0.204 \leq a \leq 0.244 \\ -142.80a^3 + 103.66a^2 - 57.76a + 6.01 & \text{for } a > 0.244 \end{cases} \quad (B.10)$$

$$A_{\max}(a) = \begin{cases} \sqrt{67.55 - 886.79a^2} - 8.22 & \text{for } a < 0.130 \\ -15.90a + 1.10 & \text{for } 0.130 \leq a \leq 0.321 \\ -4.67a^3 + 3.49a^2 - 16.70a + 1.15 & \text{for } a > 0.321 \end{cases} \quad (B.11)$$

$$a_0(Re_c) = \begin{cases} 0.57 & \text{for } Re_c < 9.5 \cdot 10^4 \\ (-9.6 \cdot 10^{-13}) (Re_c - 8.6 \cdot 10^5)^2 + 1.13 & \text{for } 9.5 \cdot 10^4 \leq Re_c \leq 8.6 \cdot 10^5 \\ 1.13 & \text{for } Re_c > 8.6 \cdot 10^5 \end{cases} \quad (B.12)$$

$$A_R(a_0) = (20 + A_{\min}(a_0)) / (A_{\min}(a_0) - A_{\max}(a_0)) \quad (B.13)$$

Therefore, the spectral function, **A**, can be finally assessed as;

$$\mathbf{A}(a) = A_{\min}(a) + A_R(a_0) [A_{\max}(a) - A_{\min}(a)] \quad (B.14)$$

The \mathbf{B} spectral function proceeds in an equal way, but $b = |\log_{10}(St_s/St_2)|$, then;

$$B_{\min}(b) = \begin{cases} \sqrt{16.89 - 886.79b^2} - 4.11 & \text{for } b < 0.130 \\ -83.61b + 8.14 & \text{for } 0.130 \leq b \leq 0.145 \\ -817.81b^3 + 355.21b^2 - 135.02b + 10.62 & \text{for } b > 0.145 \end{cases} \quad (\text{B.15})$$

$$B_{\max}(b) = \begin{cases} \sqrt{16.89 - 886.79b^2} - 4.11 & \text{for } b < 0.100 \\ -31.33b + 1.85 & \text{for } 0.100 \leq b \leq 0.187 \\ -80.54b^3 + 44.17b^2 - 39.38b + 2.34 & \text{for } b > 0.187 \end{cases} \quad (\text{B.16})$$

$$b_0(\text{Re}_c) = \begin{cases} 0.30 & \text{for } \text{Re}_c < 9.5 \cdot 10^4 \\ (-4.9 \cdot 10^{-13})(\text{Re}_c - 8.6 \cdot 10^5)^2 + 0.56 & \text{for } 9.5 \cdot 10^4 \leq \text{Re}_c \leq 8.6 \cdot 10^5 \\ 0.56 & \text{for } \text{Re}_c > 8.6 \cdot 10^5 \end{cases} \quad (\text{B.17})$$

$$B_R(b_0) = (20 + B_{\min}(b_0)) / (B_{\min}(b_0) - B_{\max}(b_0)) \quad (\text{B.18})$$

Therefore, the spectral function, \mathbf{B} , can be finally assessed as;

$$\mathbf{B}(b) = B_{\min}(b) + B_R(b_0) [B_{\max}(b) - B_{\min}(b)] \quad (\text{B.19})$$

With respect to the scale level of Eqs.(B.1), (B.2) and (B.3), the BPM model provides the following expressions;

$$K_1 = \begin{cases} -4.31 \log_{10}(\text{Re}_c) + 156.3 & \text{for } \text{Re}_c < 2.5 \cdot 10^5 \\ -9.00 \log_{10}(\text{Re}_c) + 181.6 & \text{for } 2.5 \cdot 10^5 \leq \text{Re}_c \leq 8.0 \cdot 10^5 \\ 128.6 & \text{for } \text{Re}_c > 8.0 \cdot 10^5 \end{cases} \quad (\text{B.20})$$

$$K_2 = K_1 + \begin{cases} -1000.0 & \text{for } \alpha < \gamma_0 - \gamma \\ \sqrt{\beta^2 - \left(\frac{\beta}{\gamma}\right)^2 (\alpha - \gamma) + \beta_0} & \text{for } \gamma_0 - \gamma \leq \alpha \leq \gamma_0 + \gamma \\ -12.0 & \text{for } \alpha > \gamma_0 + \gamma \end{cases} \quad (\text{B.21})$$

$$\Delta K_1 = \begin{cases} \alpha \left(1.43 \log_{10}(\text{Re}_{\delta_p^*}) - 5.29\right) & \text{for } \text{Re}_{\delta_p^*} \leq 5000 \\ 0.0 & \text{for } \text{Re}_{\delta_p^*} > 5000 \end{cases} \quad (\text{B.22})$$

ΔK_1 is the level adjustment for the pressure side contribution for non-zero angles of attack. Finally, the BPM model suggests the following expressions for γ , γ_0 , β and β_0 ;

$$\gamma = 27.09M + 3.31 \quad (\text{B.23})$$

$$\gamma_0 = 23.43M + 4.65 \quad (\text{B.24})$$

$$\beta = 72.65M + 10.74 \quad (\text{B.25})$$

$$\beta_0 = -34.19M - 13.82 \quad (\text{B.26})$$

Where, M is the local Mach number. Moreover, when the flow is not completely attached, each side of an airfoil with well-developed boundary layers produces turbulent boundary layer trailing edge noise independently of the other side. For that reason, there is a level adjustment of -3 dB at Eqs.(B.1) and (B.2) to account for equal contributions of the two surfaces to the total spectrum.

B.2 Turbulent Boundary Layer - Separation Stall Noise, TBL-SS

When the airfoil is in deep stall, separation stall noise dominates over the pressure and suction side contributions that become negligible. So, the sound pressure level is described by Eqs.(B.27), (B.28) and (B.29);

$$\text{SPL}_p[\text{dB}] = -\infty \quad (\text{B.27})$$

$$\text{SPL}_s[\text{dB}] = -\infty \quad (\text{B.28})$$

$$\text{SPL}_\alpha[\text{dB}] = 10 \log_{10} \left(\frac{\delta_s^* M^5 d \bar{D}_L}{r_e^2} \right) + \mathbf{A} \left(\frac{\text{St}_s}{\text{St}_2} \right) + K_2 \quad (\text{B.29})$$

The angle of attack in which the TBL-TE model switches, it is either the stall angle of attack of the airfoil ($\alpha = 12.5^\circ$ for the NACA0012) or the angle described by Eq.(B.24), whenever of two occurs first according to [22]. Therefore the total contribution to TBL-SS sound pressure level becomes;

$$\text{SPL}_{\text{TBL-SS}}[\text{dB}] = 10 \log_{10} \left(\underbrace{10^{\text{SPL}_p/10}}_{=0} + \underbrace{10^{\text{SPL}_s/10}}_{=0} + 10^{\text{SPL}_\alpha/10} \right) \quad (\text{B.30})$$

B.3 Laminar Boundary Layer Vortex Shedding Noise, LBL-VS

The scaling law expressed in sound pressure level for the laminar boundary layer vortex shedding is described by Eq.(B.31);

$$\text{SPL}_{\text{LBL-VS}}[\text{dB}] = 10 \log_{10} \left(\frac{\delta_p M^5 d \bar{D}_H}{r_e^2} \right) + \mathbf{G}_1 \left(\frac{\text{St}'}{\text{St}'_{\text{peak}}} \right) + \mathbf{G}_2 \left(\frac{\text{Re}_c}{(\text{Re}_c)_0} \right) + \mathbf{G}_3(\alpha) \quad (\text{B.31})$$

The length scale chosen for Eq.(B.31) is the boundary layer thickness on the pressure side due to its relevance in the phenomenon but also it gives better results than boundary layer displacement thickness. Then, the Strouhal number St' is built on a δ_p basis, therefore, it results in;

$$\text{St}' = \frac{f \delta_p}{U_e} \quad (\text{B.32})$$

The Strouhal number peak depends on the angle of attack as follows;

$$\text{St}'_{\text{peak}} = \text{St}'_1 \cdot 10^{-0.04\alpha} \quad (\text{B.33})$$

$$\text{St}'_1 = \begin{cases} 0.18 & \text{for } \text{Re}_c \leq 1.3 \cdot 10^5 \\ 0.00176 \cdot \text{Re}_c^{0.3921} & \text{for } 1.3 \cdot 10^5 < \text{Re}_c \leq 4.0 \cdot 10^5 \\ 0.28 & \text{for } \text{Re}_c > 4.0 \cdot 10^5 \end{cases} \quad (\text{B.34})$$

\mathbf{G}_1 defines the spectral shape in terms of the ratio of Strouhal number to its peak value:
 $d = St'/St'_{\text{peak}}$

$$\mathbf{G}_1(d) = \begin{cases} 39.80 \log_{10}(d) - 11.12 & \text{for } d \leq 0.597 \\ 98.41 \log_{10}(d) + 2.00 & \text{for } 0.597 < d \leq 0.854 \\ \sqrt{2.48 - 506.25 (\log_{10}(d))^2} - 5.08 & \text{for } 0.854 < d \leq 1.170 \\ -98.41 \log_{10}(d) + 2.00 & \text{for } 1.170 < d \leq 1.674 \\ -39.80 \log_{10}(d) - 11.12 & \text{for } d > 1.674 \end{cases} \quad (\text{B.35})$$

\mathbf{G}_2 function specifies the peak scaled level shape curve as a function of Reynolds number. Defining $e = Re_c/(Re_c)_0$;

$$(Re_c)_0 = \begin{cases} 10^{0.215\alpha+4.98} & \text{for } \alpha \leq 3.0 \\ 10^{0.120\alpha+5.26} & \text{for } \alpha > 3.0 \end{cases} \quad (\text{B.36})$$

$$\mathbf{G}_2(e) = \begin{cases} 77.85 \log_{10}(e) + 15.33 & \text{for } e \leq 0.324 \\ 65.19 \log_{10}(e) + 9.13 & \text{for } 0.324 < e \leq 0.569 \\ -114.05 (\log_{10}(e))^2 & \text{for } 0.569 < e \leq 1.758 \\ -65.19 \log_{10}(e) + 9.13 & \text{for } 1.758 < e \leq 3.089 \\ -77.85 \log_{10}(e) + 15.33 & \text{for } e > 3.089 \end{cases} \quad (\text{B.37})$$

\mathbf{G}_3 function introduces the angle dependence level for the shape curve of \mathbf{G}_2 ;

$$\mathbf{G}_3(\alpha) = 171.04 - 3.03\alpha \quad (\text{B.38})$$

Depending on the chord length, laminar boundary layer vortex shedding increases with the angle of attack, until a certain value is reached. Then, for higher AoA , the characteristics peaks tend to disappear and the turbulent boundary layer trailing edge noise as well as separation noise contributions dominate along the spectrum.

B.4 Trailing Edge Bluntness Vortex Shedding Noise, LBL-VS

The scaling law expressed in sound pressure level for the trailing edge bluntness vortex shedding noise is the described by Eq.(B.39).

$$\text{SPL}_{\text{TEB-VS}}[\text{dB}] = 10 \log_{10} \left(\frac{hM^{5.5}d\bar{D}_H}{r_e^2} \right) + \mathbf{G}_4 \left(\frac{h}{\delta_{\text{avg}}^*}, \Psi \right) + \mathbf{G}_5 \left(\frac{h}{\delta_{\text{avg}}^*}, \Psi, \frac{St'''}{St'''_{\text{peak}}} \right) \quad (\text{B.39})$$

In this case, the Strouhal basis is built taking, as a reference length scale, the trailing edge bluntness thickness, h ;

$$St''' = \frac{fh}{U_e} \quad (\text{B.40})$$

The peak value of Strouhal number depends on both geometric parameters: the trailing edge bluntness thickness, h , and the trailing edge solid angle, Ψ . Then:

$$St'''_{\text{peak}} = \begin{cases} \frac{0.212-0.0045\Psi}{1+0.235(h/\delta_{\text{avg}}^*)^{-1}-0.00132(h/\delta_{\text{avg}}^*)^{-2}} & \text{for } h/\delta_{\text{avg}}^* \geq 0.2 \\ 0.1(h/\delta_{\text{avg}}^*) + 0.095 - 0.00243\Psi & \text{for } h/\delta_{\text{avg}}^* < 0.2 \end{cases} \quad (\text{B.41})$$

The h/δ_{avg}^* term is the ratio of trailing edge thickness (degree of bluntness) h to the average boundary layer displacement thickness δ_{avg}^* .

$$\delta_{\text{avg}}^* = \frac{\delta_p^* + \delta_s^*}{2} \quad (\text{B.42})$$

\mathbf{G}_4 function determines the peak level of the spectrum curve. This function depends again on the geometric parameters of the airfoil;

$$\mathbf{G}_4 \left(\frac{h}{\delta_{\text{avg}}^*}, \Psi \right) = \begin{cases} 17.5 \log_{10} (h/\delta_{\text{avg}}^*) + 157.5 - 1.114\Psi & \text{for } h/\delta_{\text{avg}}^* \leq 5.0 \\ 169.7 - 1.114\Psi & \text{for } h/\delta_{\text{avg}}^* > 5.0 \end{cases} \quad (\text{B.43})$$

\mathbf{G}_5 introduces the shape of the spectrum. \mathbf{G}_5 expressions are fitted for $\Psi = 0^\circ$ and $\Psi = 14^\circ$ corresponding to the flat plate and NACA 0012 airfoil tested by [22], other values must be interpolated using Eq.(B.44).

$$\mathbf{G}_5 \left(\frac{h}{\delta_{\text{avg}}^*}, \Psi, \frac{\text{St}'''}{\text{St}_{\text{peak}}'''} \right) = \mathbf{G}_5|_{\Psi=0^\circ} + 0.0714\Psi (\mathbf{G}_5|_{\Psi=14^\circ} - \mathbf{G}_5|_{\Psi=0^\circ}) \quad (\text{B.44})$$

Where;

$$\mathbf{G}_5|_{\Psi=14^\circ} = \begin{cases} m\eta + k & \text{for } \eta < \eta_0 \\ 2.5\sqrt{1 - \left(\frac{\eta}{\mu}\right)^2} - 2.5 & \text{for } \eta_0 \leq \eta < 0 \\ \sqrt{1.563 - 1194.990\eta^2} - 125 & \text{for } 0 \leq \eta < 0.036 \\ -155.543\eta + 4.375 & \text{for } \eta \geq 0.036 \end{cases} \quad (\text{B.45})$$

$$\eta = \log_{10} (\text{St}''' / \text{St}_{\text{peak}}''') \quad (\text{B.46})$$

$$\mu = \begin{cases} 0.122 & \text{for } h/\delta_{\text{avg}}^* < 0.25 \\ -0.218 (h/\delta_{\text{avg}}^*) + 0.176 & \text{for } 0.25 \leq h/\delta_{\text{avg}}^* < 0.62 \\ -0.301 (h/\delta_{\text{avg}}^*) + 0.060 & \text{for } 0.62 \leq h/\delta_{\text{avg}}^* < 1.15 \\ 0.024 & \text{for } h/\delta_{\text{avg}}^* \geq 1.15 \end{cases} \quad (\text{B.47})$$

$$m = \begin{cases} 0.0 & \text{for } h/\delta_{\text{avg}}^* \leq 0.02 \\ 68.72 \log_{10} (h/\delta_{\text{avg}}^*) & \text{for } 0.02 < h/\delta_{\text{avg}}^* \leq 0.50 \\ 308.48 (h/\delta_{\text{avg}}^*) - 121.23 & \text{for } 0.50 < h/\delta_{\text{avg}}^* \leq 0.62 \\ 224.81 (h/\delta_{\text{avg}}^*) - 69.35 & \text{for } 0.62 < h/\delta_{\text{avg}}^* \leq 1.15 \\ 1583.28 (h/\delta_{\text{avg}}^*) - 1631.59 & \text{for } 1.15 < h/\delta_{\text{avg}}^* \leq 1.20 \\ 268.34 & \text{for } h/\delta_{\text{avg}}^* > 1.20 \end{cases} \quad (\text{B.48})$$

$$\eta_0 = -\sqrt{\frac{m^2\mu^4}{6.25 + m^2\mu^2}} \quad (\text{B.49})$$

$$k = 2.5\sqrt{1 - \left(\frac{\eta_0}{\mu}\right)^2} - 2.5 - m\eta_0 \quad (\text{B.50})$$

The $\mathbf{G}_5|_{\Psi=0^\circ}$ spectrum is obtained by computing the previous equations as one would do for $\mathbf{G}_5|_{\Psi=14^\circ}$ but replacing h/δ_{avg}^* by $(h/\delta_{\text{avg}}^*)'$. The relation between them is given by Eq.(B.51);

$$(h/\delta_{\text{avg}}^*)' = 6.724 (h/\delta_{\text{avg}}^*)^2 - 4.019 (h/\delta_{\text{avg}}^*) + 1.107 \quad (\text{B.51})$$

DTU Wind Energy is a department of the Technical University of Denmark with a unique integration of research, education, innovation and public/private sector consulting in the field of wind energy. Our activities develop new opportunities and technology for the global and Danish exploitation of wind energy. Research focuses on key technical-scientific fields, which are central for the development, innovation and use of wind energy and provides the basis for advanced education at the education.

We have more than 240 staff members of which approximately 60 are PhD students. Research is conducted within nine research programmes organized into three main topics: Wind energy systems, Wind turbine technology and Basics for wind energy.

Danmarks Tekniske Universitet

DTU Vindenergi

Nils Koppels Allé

Bygning 403

2800 Kgs. Lyngby

Telefon 45 25 25 25

info@vindenergi.dtu.dk

www.vindenergi.dtu.dk